



LAWRENCE  
LIVERMORE  
NATIONAL  
LABORATORY

# Simulations of Arctic Mixed-Phase Clouds in Forecasts with CAM3 and AM2 for M-PACE

S. Xie, J. Boyle, S. Klein, X. Liu, S. Ghan

July 26, 2007

Journal of Geophysical Research

## **Disclaimer**

---

This document was prepared as an account of work sponsored by an agency of the United States government. Neither the United States government nor Lawrence Livermore National Security, LLC, nor any of their employees makes any warranty, expressed or implied, or assumes any legal liability or responsibility for the accuracy, completeness, or usefulness of any information, apparatus, product, or process disclosed, or represents that its use would not infringe privately owned rights. Reference herein to any specific commercial product, process, or service by trade name, trademark, manufacturer, or otherwise does not necessarily constitute or imply its endorsement, recommendation, or favoring by the United States government or Lawrence Livermore National Security, LLC. The views and opinions of authors expressed herein do not necessarily state or reflect those of the United States government or Lawrence Livermore National Security, LLC, and shall not be used for advertising or product endorsement purposes.

1  
2  
3  
4  
5  
6  
7  
8  
9  
10  
11  
12  
13  
14  
15  
16  
17  
18  
19  
20  
21  
22  
23  
24

UCRL-JRNL-233107

**Simulations of Arctic Mixed-Phase Clouds in Forecasts with CAM3 and AM2  
for M-PACE**

*Shaocheng Xie, James Boyle, Stephen A. Klein,  
Lawrence Livermore National Laboratory, Livermore, California, USA*

*Xiaohong Liu and Steven Ghan  
Pacific Northwest National Laboratory  
Richland, Washington, USA*

Submitted to: *Journal of Geophysical Research*

Submission Date: 07/26/2007

Manuscript No: 2007JD009225

Revised: 11/20/2007

## Abstract

1  
2 Simulations of mixed-phase clouds in forecasts with the NCAR Atmosphere Model  
3 version 3 (CAM3) and the GFDL Atmospheric Model version 2 (AM2) for the Mixed-Phase  
4 Arctic Cloud Experiment (M-PACE) are performed using analysis data from numerical weather  
5 prediction centers. CAM3 significantly underestimates the observed boundary layer mixed-phase  
6 cloud fraction and cannot realistically simulate the variations of liquid water fraction with  
7 temperature and cloud height due to its oversimplified cloud microphysical scheme. In contrast,  
8 AM2 reasonably reproduces the observed boundary layer cloud fraction while its clouds contain  
9 much less cloud condensate than CAM3 and the observations. The simulation of the boundary  
10 layer mixed-phase clouds and their microphysical properties is considerably improved in CAM3  
11 when a new physically based cloud microphysical scheme is used (CAM3LIU). The new scheme  
12 also leads to an improved simulation of the surface and top of the atmosphere longwave radiative  
13 fluxes.

14 Sensitivity tests show that these results are not sensitive to the analysis data used for  
15 model initialization. Increasing model horizontal resolution helps capture the subgrid-scale  
16 features in Arctic frontal clouds but does not help improve the simulation of the single-layer  
17 boundary layer clouds. AM2 simulated cloud fraction and LWP are sensitive to the change in  
18 cloud ice number concentrations used in the Wegener-Bergeron-Findeisen process while  
19 CAM3LIU only shows moderate sensitivity in its cloud fields to this change. This paper shows  
20 that the Wegener-Bergeron-Findeisen process is important for these models to correctly simulate  
21 the observed features of mixed-phase clouds.

## 1 **1. Introduction**

2           Clouds have a significant impact on the surface energy budget through modulating  
3 radiative fluxes. Observations indicate that during cold seasons, mixed-phase clouds dominate  
4 low-level Arctic clouds. The radiative properties of mixed-phase clouds are largely determined  
5 by their microphysical properties, such as cloud liquid water and ice content and number  
6 concentration. Ice generally has a much larger effective radius and therefore a much smaller  
7 optical depth for a given cloud water path compared to cloud liquid water. Thus, accurate  
8 representation of the microphysical properties of mixed-phase clouds is critical for climate  
9 models to correctly simulate cloud-radiative effects in the Arctic. Earlier studies showed that the  
10 phase partitioning between cloud liquid and cloud ice in mixed-phase clouds could have a large  
11 impact on the model predicted climate change [*Li and Le Treut 1993; Gregory and Morris*  
12 *1996*].

13           However, the treatment of mixed-phase clouds in most current climate models is often  
14 oversimplified because the detailed microphysical processes involved in mixed-phase clouds are  
15 not completely understood due to the paucity of cloud observations, which is particularly true in  
16 the Arctic, and our poor theoretical understanding of fundamental thermodynamical processes in  
17 mixed phase clouds. As a result, many important microphysical processes in mixed-phase  
18 clouds, such as ice nucleation and growth and the complex interaction between the ice and liquid  
19 phases of cloud condensate, are not appropriately represented in these models. For example,  
20 some climate models still use a single-moment microphysical scheme that only predicts the  
21 mixing ratio of cloud condensate. The effective radius of cloud liquid droplets is prescribed. The  
22 effective radius of ice and the distinction between cloud liquid water and ice are usually assumed  
23 as a simple function of temperature. These simplified and/or empirically based microphysical  
24 parameterizations have largely limited the ability of these climate models to accurately simulate  
25 the evolution of mixed-phase clouds and their radiative properties [*Curry et al. 1996; Curry et al.*  
26 *2000; ACIA 2004; Vavrus 2004*]. It is also difficult to represent aerosol-cloud coupling in these  
27 models, which requires a prognostic equation for the number concentration of cloud droplets so  
28 that the impact of aerosols on the number concentration of cloud droplets can be realistically  
29 represented. The aerosol-cloud-radiation interaction is one of the key processes that is missing in  
30 many climate models. Every major climate model is adding (if they have not done this already)  
31 this interaction [e.g., *Morrison and Gettelman 2007, Gettelman et al. 2007*].

1           Improving mixed-phase cloud parameterizations requires an advanced understanding of  
2 cloud and cloud microphysics through carefully planned field studies. In recent years, several  
3 major field experiments have been conducted in the Arctic to collect the needed data for model  
4 evaluations and improvements. Examples of these field experiments include the Surface Heat  
5 Budget of the Arctic Ocean (SHEBA) project [*Perovich et al.* 1999; *Uttal et al.* 2002], the First  
6 International Satellite Cloud Climatology Project (ISCCP) Regional Experiment (FIRE) Arctic  
7 Clouds Experiment (ACE) [*Curry et al.* 2000], and the Mixed-Phase Arctic Cloud Experiment  
8 (M-PACE) [*Verlinde et al.* 2007]. Detailed in-situ observations of Arctic clouds and their  
9 microphysical properties have been obtained by using various ground based remote sensors and  
10 aircraft in these field campaigns, which provide extremely valuable information to assess and  
11 improve model cloud parameterizations.

12           Direct comparison between climate model simulations and field experiment observations  
13 is difficult because climate simulations represent statistics of the atmospheric evolution and are  
14 not initialized to any specific time observed during the field campaigns. In order to make a direct  
15 model-observation comparison, this study makes use of a tool developed from the Department of  
16 Energy (DOE) CCPP-ARM Parameterization Testbed (CAPT) project to initialize climate  
17 models with analysis data from Numerical Weather Prediction (NWP) center's data assimilation  
18 systems and then evaluate climate models in their short-range weather forecasts using field  
19 measurements. Here CCPP and ARM are the DOE Climate Change Prediction Program and  
20 Atmospheric Radiation Measurement Program, respectively. The CAPT approach has been  
21 proven as a useful way to understand climate model errors and facilitate model parameterization  
22 improvements [*Phillips et al.* 2004; *Xie et al.* 2004; *Boyle et al.* 2005, *Williamson et al.* 2005;  
23 *Sud et al.* 2006; *Klein et al.* 2006]. By initializing climate models with realistic atmospheric  
24 states from NWP analyses for the period where a selected field campaign was conducted under  
25 the CAPT framework, the detailed evolution of parameterized variables in short-range weather  
26 forecasts can be compared with field experiment data and model deficiencies can be linked  
27 directly with specific atmospheric processes observed during the field campaign. Running  
28 climate models in NWP mode also allows us to identify specific parameterization deficiencies  
29 before the compensation of multiple errors masks the deficiencies, as can occur in model climate  
30 simulations.

31           In this study, two major U.S. climate models, the National Center for Atmospheric

1 Research (NCAR) Community Atmospheric Model version 3 (CAM3) NCAR CAM3 and the  
2 NOAA Geophysical Fluid Dynamics Laboratory (GFDL) climate model (AM2), are tested under  
3 the CAPT framework against the data collected from the ARM M-PACE field campaign. M-  
4 PACE was conducted during the period from 5 – 22 October 2004 near the ARM North Slope of  
5 Alaska site and provided a complete set of measurements for Arctic clouds and their  
6 microphysical properties by using millimeter-wave cloud radars (MMCR), micropulse lidars,  
7 laser ceilometers, and aircraft [Verlinde *et al.*, 2007]. This study attempts to reveal potential  
8 deficiencies related to the cloud and cloud microphysical schemes used in these two climate  
9 models by a direct comparison of model results with the in-situ and remote sensing data from M-  
10 PACE. A new physically based cloud microphysical scheme is also tested in CAM3 to help  
11 understand how cloud microphysical processes affect the evolution and phase partitioning of the  
12 mixed-phase clouds. The sensitivity of the model results to initial data, model resolution, and  
13 cloud ice number concentration is discussed.

14 The manuscript is organized as follows. Section 2 briefly describes the models and model  
15 initialization procedure, with some details given on their cloud and cloud microphysical  
16 schemes. A new ice microphysical scheme for CAM3 is also described in this section. Section 3  
17 compares model results with the M-PACE observations. Section 4 shows results from the  
18 sensitivity tests. A summary of this study is given in section 5.

19

## 20 **2. Models and Model initialization**

### 21 **2.1. CAM3**

22 CAM3 is the NCAR atmospheric general circulation model (GCM) version 3. CAM3.1  
23 with its finite volume dynamic core at resolution of  $2.5^0 \times 2.5^0$  in the horizontal and 26 levels in  
24 the vertical is used in this study. There are four model levels below the boundary layer cloud top  
25 ( $\sim 850$  hPa) observed during M-PACE. Compared to its earlier versions, CAM3 incorporates  
26 significant improvements to its physical parameterizations of clouds and radiation. The treatment  
27 of cloud microphysics and cloud condensate in CAM3 is based on the prognostic cloud water  
28 formulation of *Rasch and Kristjansson* [1998, hereafter RK98] with modifications made by  
29 *Zhang et al.* [2003]. RK98 is a single-moment scheme that only predicts the mixing ratio of  
30 cloud condensate. The distinction between liquid and ice phase is made as a function of  
31 temperature. The fraction of liquid water in the total condensate is defined as:

1  
2  
3  
4  
5  
6  
7  
8  
9  
10  
11  
12  
13  
14  
15  
16  
17  
18  
19  
20  
21  
22  
23  
24  
25  
26  
27  
28  
29  
30  
31

$$\begin{aligned} f_i &= 0 && \text{if } T \leq T_{\min} \\ f_i &= (T - T_{\min}) / (T_{\max} - T_{\min}) && \text{if } T_{\min} < T < T_{\max} \\ f_i &= 1 && \text{if } T \geq T_{\max} \end{aligned} \quad (1)$$

where  $T$  is temperature,  $T_{\min} = -40^{\circ}\text{C}$ , and  $T_{\max} = -10^{\circ}\text{C}$ . Further improvements beyond RK98 include separate equations for predicting cloud ice and cloud liquid water, advection of cloud condensate by large-scale circulation, and gravitational settling of cloud ice and liquid particles [Boville *et al.* 2006]. However, Eq. (1) is still applied each time step to repartition the cloud liquid water and cloud ice. Cloud fraction in CAM3 is diagnosed for convective clouds based on convective mass flux and for stratiform clouds ( $C_s$ ) based on relative humidity (RH) outside of the convective cloud according to

$$C_s = ((\text{RH} - \text{RH}_{\min}) / (1 - \text{RH}_{\min}))^2 \quad (2)$$

RH is calculated with respect to water (RHw) for  $T > 0^{\circ}\text{C}$  and with respect to ice (RH<sub>i</sub>) for  $T < -20^{\circ}\text{C}$  and is interpolated using RHw and RH<sub>i</sub> between  $-20^{\circ}\text{C}$  and  $0^{\circ}\text{C}$ . The threshold relative humidity  $\text{RH}_{\min}$  varies with pressure. Other detailed information about CAM3 can be seen in Collins *et al.* [2006].

## 2.2. AM2

AM2 is the GFDL climate atmospheric model. The model resolution used in this study is  $2.0^{\circ} \times 2.5^{\circ}$  in horizontal and 24 levels in vertical (eight levels below 850 mb). Its cloud microphysical scheme follows Rotstayn [1997] and Rotstayn *et al.* [2000], in which two separate prognostic equations are used to predict cloud liquid and ice and the liquid/ice partitioning is determined by microphysical processes including the Wegener-Bergeron-Findeisen mechanism, i.e., ice crystals grow at the expense of liquid water [Wegener 1911; Bergeron 1935; and Findeisen 1938]. More detailed description about the AM2 cloud microphysical scheme can be found in Ming *et al.* [2007]. Rotstayn *et al.* [2000] assumed that saturation vapor pressure in mixed-phase cloud is with respect to liquid. As shown in the Eq. (5) in Rotstayn *et al.* [2000], the rate of change of cloud ice mixing ratio  $q_i$  is

$$\frac{dq_i}{dt} = \left(\frac{N_i}{\rho}\right)^{2/3} \frac{7.8q_i^{1/3}(e_{sl} - e_{si})}{\rho_i^{1/3}(A'' + B'')e_{si}} \quad (3)$$

Where  $N_i$  is the ice number concentration,  $q_i = M_i N_i / \rho$ ,  $M_i$  is the mass of an ice particle,  $\rho_i$  is ice density,  $e_{si}$  and  $e_{sl}$  are saturation vapor pressure with respect to ice and liquid, respectively,  $A''$  and  $B''$  are terms representing heat conduction and vapor diffusion. See details of this equation in *Rotstayn et al.* [2000]. The microphysical scheme used in AM2 is a single-moment scheme and its ice number is simply determined by the *Meyers et al.* [1992] parameterization. Cloud fraction in AM2 is determined by a prognostic cloud fraction scheme developed by *Tiedtke* [1993]. Further details are available from *GFDL GAMDT* [2004].

### 2.3. An improved ice microphysical scheme for CAM3

A physically based ice microphysical scheme described in *Liu et al.* [2007a] (LIU07) with slight modifications is also tested in CAM3 to help understand how cloud microphysical processes affect the cloud evolution and cloud ice growth in the mixed-phase clouds. LIU07 was shown to produce a more realistic simulation of the cloud phase structure and the partitioning of condensed water into liquid droplets against observations during the M-PACE than the standard SCAM when tested in the single column mode [*Liu et al.*, 2007b]. LIU07 is a double-moment scheme in which a prognostic equation is used for cloud ice number concentration together with an ice nucleation scheme developed by *Liu and Penner* [2005]. The liquid and ice mixing ratio is still calculated by the modified RK98 scheme described in *Boville et al.* [2006] but the liquid mass conversion to ice due to the deposition growth of cloud ice at the expense of liquid water (the Wegener-Bergeron-Findeisen process) is based on the *Rotstayn et al.* [2000] scheme. The original *Rotstayn et al.* [2000] scheme assumes a direct conversion from liquid to ice to maintain liquid water saturation inside in mixed-phase clouds while LIU07 assumes a conversion from water vapor to ice, which results in a smaller conversion rate of liquid to ice in mixed-phase clouds. In this study, we slightly modify LIU07 to allow a direct conversion from liquid to ice as it was assumed in the original *Rotstayn et al.* [2000] scheme but assume saturation vapor pressure  $e_w$  that is weighted by the proportions of ice and liquid water mass for mixed-phase clouds, i.e.,  $e_w = f_l * e_{sl} + (1 - f_l) * e_{si}$ , where  $f_l$  is liquid mass fraction and  $0 < f_l < 1$  in mixed phase clouds. So Eq. (3) used in CAM3LIU becomes:

$$\frac{dq_i}{dt} = \left(\frac{N_i}{\rho}\right)^{2/3} \frac{7.8q_i^{1/3}(e_{sl} - e_{si})f_l}{\rho_i^{1/3}(A'' + B'')e_{si}} \quad (4)$$

Eq. (4) yields a slower growth rate of ice mixing ratio compared to Eq. (3) because  $f_l$  is less than or equal to 1 and  $e_{sl} > e_{si}$ . It should be noted that there are debates about relative humidity in mixed-phase clouds. Based on in-situ data from FIRE-ACE and the Alliance Icing Research Study Projects [Isaac *et al.* 2001, 2005], Korolev and Isaac [2006] found that water vapor in mixed-phase clouds is close to the saturation over water (i.e.,  $f_l = 1$ ) while Fu and Hollars [2004] suggested that the water vapor pressure can be well represented by using the weighting coefficient equal to liquid fraction in the total cloud condensation based on data from the FIRE-ACE project. Korolev and Isaac [2006] explained the different conclusions between these two studies as “a result of a more detailed scheme identifying liquid and ice clouds and a more extensive handling of the corrections in the air temperature and humidity measurements” used in Korolev and Isaac [2006]. It should be noted that both assumptions about saturation vapor pressure in mixed-phase clouds are used in current microphysics parameterizations. For example, Fowler *et al.* [1996] used a weighted average of the values with respect to ice and liquid water while Rotstaysn *et al.* (2000) assumed vapor saturation with respect to liquid water as described earlier. However, addressing this issue is beyond the scope of the current study.

Another important change to CAM3 by using LIU07 is that the effective radius of cloud ice is now based on the predicted mass and number concentration of ice rather than diagnosed as a function of temperature as in the default model. This will make the computation of model radiation more sensitive to cloud properties and also impact relevant microphysical process rates like sedimentation. The stratiform cloud fraction is calculated using the same RH-based scheme with the same  $RH_{min}$  value as that in the default model except that ice super-saturation is allowed in the upper troposphere in the new scheme. As shown later, this can have an impact on simulated cloud fraction.

It is noted that both LIU07 and AM2 use the Rotstaysn *et al.* [2000] scheme for liquid water conversion to ice (Wegener-Bergeron-Findeisen process) in the mixed-phase clouds. Similar to Rotstaysn *et al.* [2000], AM2 assumes that the growth of cloud ice is at the expense of the evaporation of cloud liquid to maintain the liquid water saturation in clouds. As discussed earlier, this could result in a slightly faster conversion rate of liquid to ice in AM2 than that in the

1 slightly modified LIU07 tested in this study, which assumes that the saturation vapor pressure is  
2 weighted by the proportions of ice and liquid water mass for mixed-phase clouds. Another major  
3 difference between LIU07 and AM2 is the treatment of cloud ice number. LIU07 uses a  
4 prognostic equation to predict the ice number by considering the processes of advection,  
5 convective transport, ice nucleation, droplet freezing, microphysical conversion to precipitation,  
6 and cloud sublimation. The ice nucleation mechanisms in LIU07 include the homogeneous ice  
7 nucleation on sulfate aerosol and heterogeneous immersion nucleation on soot particles in cold  
8 clouds with temperature less than  $-35^{\circ}\text{C}$  [Liu and Penner, 2005]. In mixed-phase clouds with  
9 temperatures between  $-40^{\circ}$  and  $-3^{\circ}\text{C}$ , contact freezing of cloud droplets through the Brownian  
10 coagulation with insoluble ice nucleation is considered. Contact ice nuclei are assumed to be  
11 mineral dust [Lohmann, 2002]. Deposition/condensation ice nucleation is parameterized  
12 assuming the Meyers *et al.* [1992] (see Eq. (3) in Section 4) function of ice supersaturation.  
13 Secondary ice production between  $-3$  and  $-8^{\circ}\text{C}$  is based on Cotton *et al.* [1986] for Hallett-  
14 Mossop multiplication. In contrast, the ice number in AM2 is simply determined by the Meyers  
15 *et al.* [1992] parameterization. Additional discussion on this will be given in Section 4. Other  
16 differences between LIU07 and AM2 include that LIU07 allows ice supersaturation with respect  
17 to ice while the AM2 does not.

18

## 19 **2.4. Model initialization**

20 Both CAM3 and AM2 were initialized from the NASA Data Assimilation Office (DAO)  
21 analysis data for M-PACE. More information about the DAO analyses is available at  
22 <http://gmao.gsfc.nasa.gov/>. The analysis data were interpolated from the finer-resolution  
23 reanalysis grid ( $0.5^{\circ} \times 0.5^{\circ}$ ) to the CAM3 or AM2 grid using the procedures described in Boyle *et*  
24 *al.* [2005]. These procedures used a slightly different interpolation approach for each of the  
25 dynamic state variables, i.e., horizontal winds, temperature, specific humidity and surface  
26 pressure, along with careful adjustments to account for the difference in representation of the  
27 earth's topography between models. It was judged by comparing with the sounding data  
28 collected during the experiment that the DAO analyses reasonably captured the temporal  
29 evolution and vertical structure of the observed upper-air circulation, temperature, and moisture  
30 during M-PACE. This is important since the observed cloud systems during M-PACE are largely  
31 controlled by the synoptic-scale circulation [Verlinde *et al.* 2007].

1 A series of 3-day forecasts with CAM3 and AM2 are initialized every day at 00Z from  
2 the DAO analyses for the entire period of M-PACE from 5 – 22 October 2004. The data from  
3 hours 12 to 36 of the forecasts were concatenated and averaged onto a 3-hour interval are  
4 examined in order to reduce the impact of model spin-up that may occur in the first few hours of  
5 an integration. In this forecast range, the atmospheric state is still close to the observation so that  
6 model errors can be primarily linked to deficiencies in model physics. Results at the model grid  
7 point that is closest to the ARM Barrow site (156.4W, 71.33N) are compared with the M-PACE  
8 observations. The location of the selected model grid point is (155W, 72N) for CAM3 and  
9 (156.25W, 71N) for AM2. We have examined model results at other nearby grid points and seen  
10 some spatial variations in the simulated clouds, but the spatial variations in the simulated clouds  
11 among these nearby grid points are much smaller than the differences between model  
12 simulations and the observations as shown in next section.

### 14 **3. Results**

#### 15 **3.1 Characteristics of clouds observed from M-PACE**

16 Various types of clouds that often occur in the Arctic during its transition season were  
17 observed in the M-PACE field experiment. Figure 1a shows the time-pressure cross section of  
18 observed frequency of occurrence of clouds at Barrow by integrating measurements from the  
19 ARM cloud radar and other sensors using the ARSCL (Active Remotely-Sensed Clouds  
20 Locations) algorithm [*Clothiaux et al.* 2000]. These data are originally at 10-s and 45-m time and  
21 height intervals. They are averaged to 3-hour and 25 hPa intervals to better represent clouds over  
22 a large-scale general circulation model (GCM) grid box, which usually represents an area of 200  
23 km x 200 km. One issue with the ARSCL clouds is that cloud radar tends to underestimate the  
24 cloud top heights for high-altitude clouds because it will not be able to detect cloud particles if  
25 they sufficiently small. Another issue is that cloud radar detected cloud base can be contaminated  
26 with ice precipitation. To reduce this problem, we use the ARM laser ceilometer and micropulse  
27 lidar measurements, which are usually insensitive to ice precipitation (if the concentration of  
28 precipitation particles is not sufficiently large) or clutter, to determine the cloud base. As  
29 indicated in *Clothiaux et al.* [2000], the laser ceilometers and micropulse lidar can provide quite  
30 accurate cloud base measurements.

31 Even with these uncertainties, the cloud radar and other remote sensors provide

1 extremely valuable information about the vertical distribution of various types of clouds over the  
2 ARM barrow site. During M-PACE, the ARSCL data indicated that Barrow was covered with  
3 multilayered stratus clouds in the mid- and low-levels with the cloud top up to 550 hPa for 5 – 8  
4 October, persistent single-layer boundary layer stratocumulus with the cloud top around 850 hPa  
5 during the period from 8 to 14 October, and deep prefrontal and frontal clouds (including cirrus)  
6 from 15 – 22 October.

7         The observed cloud systems were largely controlled by the synoptic-scale circulation  
8 affecting that area during M-PACE. As described in *Verlinde et al.* [2007], for the period from 5  
9 – 15 October, the North Slope of Alaska (NSA) was dominated by a strong surface high-pressure  
10 system built over the pack ice to the northeast of the Alaska coast. Associated with the strong  
11 surface high, east-northeasterly flow prevailed at low levels. The low-level northeasterly flow  
12 combined with a midlevel low pressure system drifted along the northern Alaska coast generated  
13 the complicated multilayer cloud structure over NSA from 5 – 7 October. The single-layer low-  
14 level clouds observed from 8 – 15 October originally formed over the ocean adjacent to the  
15 Alaskan coast as the low-level east-northeasterly flow brought cold near-surface air from the  
16 pack ice to the warm ocean and then advected to Barrow. Large surface turbulent fluxes are the  
17 major driver for the evolution of the boundary layer clouds. During this period, there was a  
18 substantial temperature decrease at altitudes below the 665 hPa pressure level and a sharp  
19 moisture decrease over the Barrow site. The range of cloud temperature was from  $-5^{\circ}$  C to  $-20^{\circ}$   
20 C, indicating that the cloud condensate was mixed phase. After 14 October, the boundary layer  
21 clouds started to disappear as a warm front moved through the area on 15-16 October and a deep  
22 ridge moved over the NSA. Southwesterly flow prevailed in the entire troposphere except on  
23 late 19 October when there was an abrupt wind direction change from the southwest to the  
24 southeast associated with a strong warm frontal passage which brought in deep prefrontal and  
25 frontal clouds. Cirrus clouds were seen during this period.

26         To obtain in-situ and remote sensing measurements of microphysical properties of these  
27 cloud systems, the ARM millimeter cloud radar, micropulse lidars, laser ceilometers, and two  
28 instrumented aircraft were used in the experiment. For the single-layer boundary layer clouds,  
29 data collected from both the surface-based remote sensing instruments and the aircraft revealed  
30 the presence of a maximum liquid water layer near cloud top and liquid and irregular ice crystals  
31 within the cloud layer with precipitating ice beneath the liquid cloud base [*McFarquhar et al.*

1 2007]. This result is consistent with the findings from other arctic field campaigns [*Pinto* 1998;  
2 *Hobbs and Rangno* 1998; *Curry et al.* 2000]. The multilayered clouds had a more complicated  
3 structure than the single-layer clouds. Up to six liquid cloud layers were detected by the ARM  
4 narrow-band lidar and the depth of individual liquid cloud layers varied from 50 to 300 m.  
5 Combined radar and lidar data indicated the existence of precipitating ice with low ice water  
6 content between the layers. These characteristics are similar to those from the in situ  
7 measurements by the aircraft. A detailed summary of the observed clouds during M-PACE can  
8 be seen in *Verlinde et al.* [2007] and *McFarquhar et al.* [2007]. In the following discussion, we  
9 examine how well CAM3 and AM2 capture these observed features in the arctic clouds.

### 11 **3.2 Model-simulated clouds**

12 Figures 1b, 1c, and 1d show the model-produced cloud fraction at Barrow from CAM3,  
13 AM2, and the CAM3 with the new ice microphysics described in section 2 (hereafter  
14 CAM3LIU), respectively. It should be noted that model clouds represent a fraction of a model  
15 grid box occupied by clouds, which is different from the radar and lidar detected frequency of  
16 occurrence of clouds as shown in Figure 1a. Cloud fractions in CAM3 and AM2 have to be  
17 parameterized in terms of the large-scale variables such as grid mean relative humidity because  
18 they cannot be resolved by CAM3 and AM2 with their current spatial resolutions. There is  
19 always a concern about the comparison between the model clouds and the single point radar and  
20 lidar measurements. Averaging the ARSCL clouds from the 10-s and 45-m time and height  
21 intervals onto the 3-hour and 25 hPa intervals improves the representation clouds over a GCM  
22 grid box, especially for the highly horizontally advective boundary layer clouds and frontal  
23 clouds observed during M-PACE. Nevertheless, it is still difficult to quantitatively compare  
24 model clouds with the ARSCL data. So the purpose here is to qualitatively evaluate the model  
25 clouds using the available ARM radar and lidar data and demonstrate inter-model differences in  
26 their simulated clouds.

27 Figure 1 shows that all the models are able to qualitatively reproduce the cloud types  
28 observed during M-PACE, such as the multilayered clouds from 5 – 8 October, the boundary  
29 layer clouds from 8 – 14 October, and the frontal deep high clouds from 15 – 22 October.  
30 However, there are considerable differences in detailed structures of the clouds between the  
31 observations and the model simulations. For the period 5 – 14 October, the default CAM3

1 substantially underestimates the observed multi-layered and single-layer boundary layer cloud  
2 fraction. In contrast, AM2 produces much more mid- and low-level cloud fraction than CAM3. It  
3 is interesting to see that the CAM3 with the new ice microphysics produces more realistic single-  
4 layer boundary clouds than the default CAM3 while it generates too many mid- and high level  
5 clouds. The overestimation of mid- and high level clouds is partially related to the scheme's  
6 allowance of ice supersaturation. As discussed earlier, CAM3 uses a RH-based cloud scheme to  
7 diagnose stratiform cloud fraction (Eq. (2)) and its RH is determined by a combination of ice and  
8 water saturation. Given the same threshold  $RH_{\min}$ , the new scheme would lead to more cloud  
9 fraction than the default CAM3 due to the allowance of ice supersaturation. We have found that  
10 the RH in CAM3LIU is often supersaturated with respect to ice in the mid- and high levels  
11 where temperature is usually less than  $-20^{\circ}\text{C}$  during M-PACE. One common problem for all the  
12 models is that the modeled cloud top and cloud base are lower than the observed for the period 8  
13 – 15 October. The averaged cloud [top, base] pressures over this period for ARSCL, CAM3,  
14 CAM3LIU, and AM2 are [840, 939], [855, 985], [851, 991], and [865, 1006] (hPa), respectively.  
15 This may be partially related to the coarse vertical resolutions used in these models, which  
16 cannot well resolve the observed boundary layer structure. For example, CAM3 only has four  
17 model levels below 850 hPa, the level of the observed single-layer boundary layer cloud top. For  
18 the deep frontal clouds, the models tend to overestimate the clouds at high levels and  
19 underestimate them at mid- and low levels. The problem with the mid- and low-level clouds is  
20 particularly severe for the CAM models. In addition, the model-simulated frontal clouds tend to  
21 have a longer lifetime and weaker temporal variability than the observed. This is a common  
22 problem for most large-scale models in simulating frontal clouds [e.g., *Klein and Jakob, 1999;*  
23 *Zhang et al, 2005; Xie et al. 2005*]. The temporal variability in the observed frontal clouds is  
24 partially related to subgrid-scale dynamics which cannot be resolved in large-scale models. The  
25 difference in temporal variability between the models and observations may also due to the fact  
26 that the ARM observations are from a point whereas the models are grid box averaged.

27         Figure 2 compares the total cloud fraction from the models and the total cloud frequency  
28 from the observations at Barrow. The observed total cloud frequency is calculated from the  
29 ARSCL products assuming maximum cloud overlap over a 3-hour interval. The observations  
30 typically showed a persistent almost 100% cloud cover during the period 5 – 14 October except  
31 on 7 – 8 and 11 October where the cloud cover decreased slightly. Consistent with earlier

1 discussions, CAM3 considerably underestimates the total cloud cover for this period. This  
2 problem is significantly reduced in CAM3LIU when the new physically based ice microphysical  
3 scheme is used. AM2 also produces a much better cloud cover than the default CAM3. It is seen  
4 that the cloud fraction produced by the default CAM3 shows larger temporal variability than the  
5 observations, indicating the inability to produce clouds under the same conditions as nature as  
6 the conditions change. In contrast, CAM3LIU and AM2 have 100% cloud cover for most of the  
7 period 5 – 14 October, similar to the observations. For the deep frontal clouds, both CAM3LIU  
8 and AM2 largely overestimate the observed cloud fraction while CAM3 generally agrees well  
9 with the observation.

10         Figures 3a-c show the grid box mean liquid water mixing ratio (LWC) produced from  
11 these models. The contour lines in Figure 3 are the model produced temperatures. All the models  
12 are able to produce two or more liquid cloud layers for the period 5 – 8 October even though the  
13 fine vertical structures of the observed multi-layer clouds as shown in *Verlinde et al.* [2007] are  
14 not well simulated due to the coarse model vertical resolution. In comparison with CAM3LIU,  
15 CAM3 predicts similar amount of cloud liquid water for the boundary clouds even though its  
16 cloud fraction is much lower. This is partially due to its temperature dependent liquid/ice  
17 partitioning. For the range of temperature  $-5^{\circ}\text{C} \sim -20^{\circ}\text{C}$ , the majority of cloud condensate  
18 produced in CAM3 will be liquid. Another noteworthy feature is that CAM3 has much more  
19 liquid in the mid- and upper level clouds than both CAM3LIU and AM2, which leads to a  
20 considerable overestimation of the observed liquid water path in CAM3 during these periods. It  
21 is noted that AM2-produced clouds contain much less liquid than CAM3LIU for the mixed-  
22 phase boundary clouds although they produce comparable cloud fraction and include the  
23 Wegener-Bergeron-Findeisen microphysical process. This suggests a faster conversion rate of  
24 liquid to ice in AM2 than CAM3LIU, which should be partially related to the differences in  
25 specifying the vapor saturation and the cloud ice number concentration between these two  
26 models as discussed in Section 2.2.

27         Figure 4 is the same as Figure 3 except for ice water mixing ratio. Since there is no  
28 distinction between ice and snow inside the cloud for AM2 (i.e., AM2 ice includes snow inside  
29 the cloud) but for CAM3 there is, we add model snow field to the ice water mixing ratio in  
30 CAM3 and CAM3LIU for a better comparison with AM2. For simplicity, we use “ice” to  
31 represent the sum of ice and snow in our following discussions. It should be noted that the snow

1 in CAM3 and CAM3LIU has no impact on radiation while the snow inside cloud in AM2 affects  
2 model radiation since it is treated as ice. Compared to CAM3 and CAM3LIU, AM2 produces  
3 less ice for boundary layer clouds and near the surface partially due to the fact that the snow  
4 falling out of clouds is not included in Figure 4b while it produces significantly larger ice in the  
5 strong frontal clouds on 19 October. Generally, CAM3LIU generates more ice than the default  
6 CAM3, especially for the boundary layer mixed-phase clouds.

7         Figures 5a and 5b show the observed and modeled cloud liquid water path (LWP) and  
8 cloud ice water path (IWP) at Barrow, respectively. Note that both observed and modeled IWPs  
9 include snow component since the observations cannot separate snow from ice. There are two  
10 sources for the observed LWP. Both are based on the ARM Microwave Radiometer (MWR)  
11 measurements but they are retrieved using different retrieval algorithms. One is based on the  
12 algorithm described in *Turner et al.* [2007] and another one is derived using *Wang* [2007]. The  
13 observed IWP is derived from the ARM cloud radar and lidar measurements [*Wang and Sassen,*  
14 2002]. The remote sensing retrieved IWP is currently available for the single-layer boundary  
15 layer mixed-phase clouds with an estimated error of about 50%. The uncertainty in the LWP  
16 retrieved using the algorithm from *Turner et al.* [2007] is about  $15 - 25 \text{ g m}^{-2}$  for clouds of any  
17 liquid water path and it is about  $6 \text{ g m}^{-2}$  based on the uncertainty estimated in the *Wang* [2007]  
18 retrieved LWP for clouds with LWP up to  $40 \text{ g m}^{-2}$  (there is no uncertainty estimate for *Wang's*  
19 data for the M-PACE period where cloud LWP is usually larger than  $100 \text{ g m}^{-2}$ ). It is seen that  
20 the LWPs from these two measurements agree with each other very well for the period when the  
21 radar and lidar retrievals are available. CAM3 reasonably reproduces the observed LWP for the  
22 single-layer mixed phase clouds even though its cloud amount is significantly smaller than the  
23 observations. This inconsistency between LWP and cloud fraction in CAM3 is due to the fact  
24 that CAM3 cloud fraction is determined by its large-scale relative humidity rather than its cloud  
25 condensate. One clear problem with the default CAM3 is that it largely overestimates the  
26 observed LWP for the mid- and high level clouds (e.g., Oct. 7, 16, 18 – 20). This problem is  
27 significantly reduced with the use of the new ice microphysical scheme as shown in CAM3LIU,  
28 which also predicts a reasonable LWP for the boundary layer clouds. Consistent with earlier  
29 discussion, the LWP in AM2 is considerably smaller than the CAM models and the observations  
30 for the boundary layer clouds, suggesting the conversion rate of liquid to ice might be too fast in  
31 AM2. However, it is surprising to see that the single-layer boundary layer clouds produced by

1 AM2 do not have much ice either. Further sensitivity tests with its microphysical scheme are  
2 needed to fully understand this inconsistency. For the frontal clouds occurring during 15 – 22  
3 October, the IWPs simulated by CAM3 and CAM3LIU agree with each very well while AM2  
4 produces significantly larger IWP than CAM3 for the strong deep frontal clouds on 19 October,  
5 which suggests more rapid glaciations occurred in AM2 than the CAM models for the deep  
6 frontal clouds.

7 To better understand the large differences in the simulated cloud fields among these  
8 models, we examine the model simulated surface turbulent fluxes, which are largely responsible  
9 for driving the evolution of the boundary layer clouds for the period Oct. 9 -14. Since the clouds  
10 observed at Barrow originally advected from the ocean adjacent to the Alaskan coast, we  
11 examine the model results at an upwind model grid point. The location of this selected upwind  
12 model grid point is (152.5W, 72N) for CAM3 and CAM3LIU and (153.75W, 73N) for AM2.  
13 Over Oct. 9 – 14, AM2 has slightly larger sensible and latent heat fluxes than CAM3 and  
14 CAM3LIU. The average sensible heat flux over this period is  $146 \text{ W m}^{-2}$  for AM2,  $123 \text{ W m}^{-2}$   
15 for CAM3, and  $129 \text{ W m}^{-2}$  for CAM3LIU and the average latent heat flux is  $99 \text{ W m}^{-2}$  for AM2,  
16  $87 \text{ W m}^{-2}$  for CAM3, and  $85 \text{ W m}^{-2}$  for CAM3LIU. The slightly larger heat fluxes in AM2  
17 might partially lead to a larger cloud fraction compared to the default CAM3. However, the large  
18 differences shown in the CAM3 and CAM3LIU produced cloud fraction and cloud properties  
19 cannot be easily explained by their surface turbulent fluxes, which are very similar for these two  
20 models. This suggests that the differences shown in the CAM3 and CAM3LIU simulated clouds  
21 are mainly due to the different microphysical parameterizations used in these two models. Over  
22 the period, AM2 also produces a slightly larger surface precipitation rates than CAM3 and  
23 CAMLIU. The average surface precipitation rates at Barrow are  $0.7 \text{ mm day}^{-1}$  for AM2,  $0.43$   
24  $\text{mm day}^{-1}$  for CAM3, and  $0.42 \text{ mm day}^{-1}$  for CAM3LIU.

25

### 26 **3.3 Microphysical properties in the single-layer mixed-phase clouds: model vs. aircraft data**

27 During M-PACE, there were four flights conducted on Oct. 9 -12 to obtain cloud  
28 properties in the single-layer boundary layer mixed-phase clouds. Each flight lasted one or two  
29 hours with cloud data collected every 10 seconds. While these in-situ aircraft data provided  
30 unique information to understand the microphysical properties in the mixed-phase clouds, it is  
31 difficult to use them to quantitatively compare with model results because the mismatches

1 between them. For example, the model outputs are at a much lower temporal and spatial  
2 resolution (representing a mean over 3 hour and an area of 200km x 200km) than the aircraft  
3 measurements (10 seconds, point measurements). So our purpose here is to see if these models  
4 can reproduce qualitatively well some important statistical features revealed by the aircraft data.  
5 In the following Figures (6 and 7), a cloud is defined when the total cloud condensate is larger  
6 than  $0.001 \text{ g m}^{-3}$  for both model results and in-situ measurements. To improve statistics, the  
7 model data used in Figures 6 and 7 are for the entire period from 9 – 14 October when the single  
8 layer boundary layer clouds are generated in these models.

9 Figure 6a displays the liquid fraction ( $f_l$ ) in the total cloud condensate as a function of  
10 height measured by the University of North Dakota (UND) Citation from the four flights  
11 conducted on 9 – 12 October for the single-layer mixed-phase clouds. The 10s raw aircraft data  
12 were processed by *McFarquhar et al.* [2007]. The cloud altitude is normalized from 0 at liquid  
13 cloud base to 1 at cloud top. The different color dots in Figure 6a represent data collected from  
14 different flights. The aircraft data revealed the dominance of cloud liquid water in the boundary  
15 layer mixed-phase clouds with 79% of cases having  $f_l > 90\%$ . In general,  $f_l$  increases with height  
16 and is larger than 80% near cloud top. It is important to notice that many data points with low  $f_l$   
17 are found in the lower half of the cloud, indicating the presence of significant amounts of ice.  
18 The strong liquid layer near cloud top leads to strong cloud-top radiative cooling, which may  
19 play an important role in maintaining the persistence of mixed-phase boundary layer clouds [e.g.,  
20 *Pinto, 1998*].

21 Figures 6b-6d is the same as Figure 6a except for CAM3, AM2, and CAM3LIU,  
22 respectively. The snow component is added to the total cloud condensate when the modeled  
23 liquid fraction is calculated in order to be consistent with the aircraft measurements processed by  
24 *McFarquhar et al.* [2007], which include all particles greater than  $53 \mu\text{m}$ . This observed vertical  
25 distribution of  $f_l$  is clearly not reproduced by CAM3 in which  $f_l$  generally decreases with height  
26 due to its temperature dependence. The few points with low  $f_l$  found at the cloud base in Figure  
27 6b are due to the model-produced snow. In contrast, the observed variation of liquid water  
28 fraction with cloud height is reasonably captured by CAM3LIU. AM2 also shows a better  
29 agreement with the observations than CAM3. The lack of low  $f_l$  points near the cloud base in  
30 AM2 is probably due to the fact that the snow falling out of the cloud is not included in the AM2  
31 total cloud condensate when  $f_l$  is calculated.

1 Figure 7a shows the measured  $f_l$  as a function of temperature from the same flights as  
2 Figure 6a. The measured cloud temperatures during these flights are about between  $-16^{\circ}\text{C}$  to -  
3  $9^{\circ}\text{C}$ . It is seen that there is no clear relationship between  $f_l$  and temperature in the observations.  
4 Significant amounts of liquid and ice co-exist within this temperature range. It is obvious that  
5 any temperature based liquid/ice partitioning schemes will fail to reproduce the observed  
6 structure, such as the scheme used in CAM3 (see Figure 7b). Once again, AM2 and CAM3LIU  
7 reasonably reproduce the observed variation with temperature of  $f_l$  by including the Wegener-  
8 Bergeron-Findeisen process (Figures 7c-d). This indicates that the Wegener-Bergeron-Findeisen  
9 process is critical for the models to correctly capture observed structure of cloud condensate in  
10 the mixed-phase clouds.

### 11 12 **3.4 Radiation**

13 Clouds have a large impact on surface radiation. However, it is difficult to evaluate  
14 model shortwave radiation (SW) with point measurements taken at a station located near the  
15 coast (e.g., Barrow). The closest CAM and AM2 model output grid points to the Barrow site  
16 cover both ocean and land areas, over which the surface characteristics are very different. For  
17 example, there is a very strong contrast in the surface albedo between ocean and land. During M-  
18 PACE, the ARM Barrow site was covered by snow with the surface albedo in a range of 0.7 to  
19 0.9 [Xie *et al.* 2006] while its nearby ocean was open water, which had much smaller surface  
20 albedo (less than 0.2). The difference in the surface albedo between the models and the  
21 observations makes it difficult to interpret model-observation comparison since surface albedo  
22 has a large impact on both the surface upward and downward radiation, in addition to clouds.  
23 Thus, in this study we will focus our discussion on the surface downward longwave radiation and  
24 the top of the atmosphere (TOA) outgoing longwave radiation, which are more related to clouds  
25 and less dependent on surface conditions. Moreover, longwave radiative fluxes are the dominant  
26 terms in the surface and TOA energy budgets in the cold Arctic season.

27 Figure 8a displays the observed and modeled downward longwave radiative fluxes (LW)  
28 at surface. The observed surface radiation data are obtained from the ARM Solar and Infrared  
29 Radiation Station. For the period 5 – 14 October, the observed surface downward LW shows a  
30 rather weak temporal variability due to the presence of persistent low-level clouds. The observed  
31 value is significantly underestimated by CAM3, due primarily to its underestimation of the low-

1 level clouds as shown in Figures 1 and 2. In addition, CAM3 shows much larger temporal  
2 variation in the surface downward LW than the observations, consistent with the larger temporal  
3 variation in its produced cloud cover (Figure 2). These problems are largely reduced in  
4 CAM3LIU, which only slightly overestimates the observations for the period 10 -14 October.  
5 The overestimation may be related to the lower cloud base altitude in CAM3LIU. AM2 also  
6 shows a better simulation of the surface downward LW than CAM3. Its surface downward LW  
7 agrees well with the observations for most of the period while it significantly underestimates the  
8 observations on Days 9, 13, and 14 associated with the problem with its simulated cloud field.  
9 The averaged surface downward LW fluxes over the period 5 – 14 October are 284, 264, 291,  
10 and 278 (W/m<sup>2</sup>) for the observations, CAM3, CAM3LIU, and AM2, respectively. For the period  
11 15 – 22 October, all the models generally overestimate the observed surface downward LW,  
12 partially due to the longer lifetime for the frontal clouds simulated by these models.

13 Figure 8b is the same as Figure 8a except for the outgoing longwave radiative fluxes  
14 (OLR) at top of the atmosphere. The observed TOA radiative fluxes are from the 1<sup>0</sup> x 1<sup>0</sup> analysis  
15 of the NASA Terra and NOAA 16 satellite measurements. All the models consistently  
16 overestimate the observed OLR in the presence of the single-layer boundary layer clouds (9 -14  
17 October). This is related to the underestimation of the cloud fraction and cloud liquid water path  
18 during this period as discussed earlier. The model underestimation of the low-level cloud top  
19 altitude may also contribute to this problem. Compared to CAM3, the overestimation is largely  
20 reduced in CAM3LIU. It is seen that CAM3LIU considerably underestimates the observed OLR  
21 on day 7 when the multi-layered clouds occurred. This is mainly because CAM3LIU clouds  
22 extend to much higher altitude (300 hPa) than the observed (~ 550 hPa) (see Figure 1). For the  
23 deep frontal period, the smaller OLR produced by the models on 15-16 October and 17-18  
24 October is consistent with the higher frontal cloud fraction generated by these models compared  
25 to the observations.

26

#### 27 **4. Sensitivity tests**

28 Several sensitivity tests are conducted to illustrate how sensitive model results are to  
29 initial data, model resolution, and cloud ice number concentration. As mentioned earlier, the  
30 CAPT approach is to initialize a climate model with the NWP analyses without developing its  
31 own data assimilation system. Since the NWP analyses are not perfect and are affected by

1 deficiencies in the model used to produce the analysis, model results may be sensitive to the  
 2 analyses from different NWP centers. Thus, it is useful to examine if the model behaviors shown  
 3 in this study are robust and not dependent on a particular analysis. For this purpose, we tested  
 4 CAM3 and CAM3LIU with the National Center for Environmental Prediction (NCEP) Global  
 5 Data Assimilation System (GDAS) analysis data (<http://wwwt.emc.ncep.noaa.gov/gmb/gdas/>)  
 6 for M-PACE. Similar to the DAO analyses, the GDAS analyses also reasonably represent the  
 7 observed atmosphere for M-PACE but with slightly smaller biases of generally less than 1 K in  
 8 temperature and 0.1 g/kg in moisture compared to the errors of less than 1.5 K in temperature  
 9 and 0.1 g/kg in moisture in the DAO analyses. We found that the forecasts of clouds and cloud  
 10 microphysical properties with the GDAS data are very similar to those with the DAO analyses as  
 11 shown in Section 3. This indicates that the errors associated with the simulated mixed-phase  
 12 clouds in CAM3 and the improvements seen in CAM3LIU with the new ice microphysical  
 13 scheme are rather robust with respect to conditions with initial data.

14 Another two sensitivity tests were conducted with AM2: AM2N90 is AM2 with a higher  
 15 horizontal resolution of  $1.0^{\circ} \times 1.25^{\circ}$  and AM2N90N is the same as AM2N90 but with a modified  
 16 parameterization of ice number density based on the M-PACE ice nuclei (IN) observations. As  
 17 described in Section 2.2, AM2 uses a parameterization of the Wegener-Bergeron-Findeisen  
 18 process based upon *Rotstayn et al.* [2000]. The parameterization is based upon the diffusional  
 19 growth of ice in the presence of liquid drops that maintain the ambient water vapor at liquid  
 20 water saturation (and thus ice-supersaturation). The rate of change of the ice mixing ratio is  
 21 proportional to the assumed number density of ice. Since AM2 does not have a prognostic  
 22 equation for the number density of ice, this is parameterized following *Meyers et al.* [1992]:

$$23$$

$$24 \quad N_i = \exp[12.96(e_{sl} - e_{si})/e_{si} - 0.639] \quad (5)$$

$$25$$

26 Where  $N_i$  ( $L^{-1}$ ) is the ice number concentration,  $e_{sl}$  is the saturation vapor pressure of liquid, and  
 27  $e_{si}$  is the ice saturation vapor pressure. The constant parameters used in Eq. (5) are empirically  
 28 determined from mid-latitude measurement of ice nuclei (IN) concentrations for the temperature  
 29 range from  $-7^{\circ}C$  to  $-20^{\circ}C$ , which are generally much higher than Arctic IN concentrations [e.g.,  
 30 *Bigg*, 1996]. In order to best fit M-PACE observations of ice nuclei, *Prenni et al.* [2007]  
 31 modified Eq. (5) to

1  
2 
$$N_i = \exp[1.87(e_{sl} - e_{si})/e_{si} - 1.488] \quad (6)$$
  
3

4 In the sensitivity study (AM2N90N), Eq. (6) is used to calculate the ice number density  
5 used in the parameterization of the Wegener-Bergeron-Findeisen process. At the typical  
6 temperature range of M-PACE clouds ( $-10^0\text{C}$  to  $-15^0\text{C}$ ), Eq. (6) results in a much smaller ice  
7 number density of  $0.29 \text{ L}^{-1}$  as compared to  $3.23 \text{ L}^{-1}$  from Eq. (5).

8 The ice nuclei (IN) concentrations used to obtain Eq. (6) were obtained from the  
9 measurements of a Continuous Flow Diffusion Chamber (CFDC) aboard the Citation aircraft  
10 used in M-PACE. The CFDC measurements represent the total number concentration of active  
11 IN that have diameters less than  $2 \mu\text{m}$  acting in deposition, condensation, and immersion-  
12 freezing modes (without contact freezing). The CFDC IN concentrations are often dramatically  
13 different from the ice crystal number concentrations measured by the cloud probes (e.g., one- or  
14 two-dimensional cloud probes and the Forward Scattering Spectrometer Probe). For the flights  
15 taken on 9 – 10 October for the single-layer mixed phase clouds, the CFDC measured IN vary  
16 from  $0.1$  to  $1 \text{ L}^{-1}$ , which are considerably lower than the ice crystal number concentrations  
17 measured by the cloud probes, which generally vary from  $0.1$  to  $10 \text{ L}^{-1}$  with an average of  $2.8 \text{ L}^{-1}$   
18 and a standard deviation of  $6.9 \text{ L}^{-1}$  [McFarquhar *et al.*, 2007]. Using the CFDC measured IN,  
19 current known ice nucleation processes are not able to reproduce the M-PACE observed ice  
20 crystal number concentrations, which often exceed the total amount of ice nucleated by at least  
21 an order of magnitude [Fridlind *et al.* 2007]. Fridlind *et al.* [2007] suggested that this  
22 discrepancy could be due to some additional ice initiation mechanisms that are not parameterized  
23 in current numerical models and not detected by the CFDC. Based on their large-eddy  
24 simulations with size resolved microphysics for M-PACE, Fridlind *et al.* [2007] found that the  
25 processes previously hypothesized to explain the discrepancy, such as shattering of drops during  
26 freezing and fragmentation during ice-ice collisions, are not able to account for the difference.  
27 They further found that the two additional ice initiation processes, formation of ice nuclei from  
28 drop evaporation residuals and drop freezing during evaporation, could be strong enough to  
29 account for the observed ice crystal number concentration.

30 Figures 9a displays the simulated cloud fraction from AM2N90 at the model grid point  
31 ( $155.625\text{W}$ ,  $71.5\text{N}$ ) closest to Barrow for M-PACE. Compared to the default AM2, AM2N90

1 produces slightly smaller cloud fraction for the multilayered and single-layer boundary layer  
2 clouds. The mid-level clouds from Oct. 5-8 are not well captured by AM2N90. As one can  
3 expect that the observed temporal variability in deep frontal clouds from Oct. 15-22 is better  
4 reproduced in AM2N90 since the frontal scale circulations are better resolved with increasing the  
5 model horizontal resolution. It is seen that AM2N90-produced clouds contain slightly more  
6 liquid water than AM2-simulated, but they are still less than the observations (Figure 10a). The  
7 IWP produced by AM2N90 is very similar to that in AM2 (Figure 10b).

8 Earlier studies have shown that the concentration of ice crystals plays very important role  
9 in maintaining mixed-phase clouds in Arctic [*Pinto, 1998; Harrington et al. 1999; Jiang et al.*  
10 *2000*]. Using a single-column model coupled to a bulk microphysics parameterization to  
11 simulate clouds observed at SHEBA, *Morrison et al. [2003]* indicated that the model simulated  
12 liquid cloud fraction and LWP are very sensitive to uncertainties in the ice number concentration  
13 while IWP exhibits comparatively less sensitivity. Consistent with these previous studies, the  
14 AM2 simulated clouds and cloud properties also exhibit quite large sensitive to the change in the  
15 parameterization of ice number concentration. In general, the smaller ice number density used in  
16 AM2N90N leads to a significant increase in both cloud fraction (Figure 9b) and cloud liquid  
17 water path for the period Oct. 6 -15 (Figure 10a) while there is only a small change in the  
18 simulated cloud ice in comparison with AM2N90 (Figure 10b). It is noteworthy that the  
19 AM2N90N simulated multi-level and boundary layer clouds are higher in altitude and more  
20 close to the observations than AM2N90.

21 It should be noted that the diagnosed  $N_i$  based on the IN observed from the CFDC in the  
22 AM2N90N test is much smaller than the M-PACE observed value ( $0.29 \text{ L}^{-1}$  vs.  $2.8 \text{ L}^{-1}$ ). An  
23 overall better performance obtained by AM2N90N compared to AM2N90 that used a  $N_i$  closer to  
24 the observation ( $3.23 \text{ L}^{-1}$  vs.  $2.8 \text{ L}^{-1}$ ) may indicate either the measured ice crystal number  
25 concentrations are too large or there are potential problems with the model microphysics  
26 parameterizations, i.e., the better results are just for wrong reasons. It is known that the observed  
27 ice crystal number concentrations may be slightly overestimated due to ice breakup on aircraft  
28 instruments and the CFDC detected IN number concentrations are underestimated by some  
29 amount by excluding aerosols larger than  $2 \mu\text{m}$  and contact-mode nucleation. However, these  
30 errors cannot fully explain the large discrepancy between these two measurements. As suggested  
31 by *Fridlind et al. [2007]*, the large discrepancy could be because some additional ice initiation

1 mechanisms are missing in current parameterizations of ice nucleation processes and are not  
2 detected by the CFDC. If we trust the measured ice crystal number concentrations during M-  
3 PACE, the worse results from AM2N90 might suggest potential deficiencies with its  
4 microphysics scheme. For example, the conversion rate from liquid to ice may be too fast in  
5 AM2 because the model significantly underestimates the observed LWP for the mixed-phase  
6 clouds if it uses an ice number concentration that is close to the M-PACE observations. Using a  
7 lower IN concentration in AM2N90N increases LWP, thus improve the model prediction. The  
8 large sensitivity of the model cloud fraction and LWP to uncertainties in the ice number  
9 concentrations shown in the AM2N90N test indicates the importance of correctly representing  
10 this field in AM2. It also suggests that more accurate measurements of IN and ice crystal number  
11 concentrations are required to guide future model microphysics parameterization developments.

12         Similar to the AM2N90N sensitivity test, we applied the CFDC measured IN (Eq. (6)) to  
13 CAM3LIU to represent deposition/condensation ice nucleation in its ice-phase microphysical  
14 scheme. This leads to a much smaller ice number concentration of  $0.44 \text{ L}^{-1}$  compared to  $2.74 \text{ L}^{-1}$   
15 from using Eq. (5) over the flight periods on Oct. 9 – 10. Figure 11 shows the simulated cloud  
16 fraction from CAM3LIU with the CFDC measured IN (CAM3LIUN) for M-PACE. In contrast  
17 to the AM2N90N test, the simulated cloud fraction in CAM3LIU is not sensitive to the change in  
18 the ice nuclei number concentration. One likely reason is that cloud fraction in CAM3 is not  
19 closely linked to its cloud condensate, but rather is more dependent on its large-scale relative  
20 humidity as discussed earlier. Similar to the AM2N90N test, the smaller ice number  
21 concentration in CAM3LIUN results in larger LWP, especially for the single-layer boundary  
22 layer mixed-phase clouds observed on Oct. 9 – 14 (Figure 12a), but the change is not that  
23 dramatic as that shown in the AM2N90N test (Figure 10a). For the same period, CAM3LIUN  
24 produced smaller IWP than CAM3LIU and the remote sensing retrieved value. Overall, the  
25 performance of CAM3LIUN in its simulated clouds is similar to CAM3LIU. This is also  
26 different from the results obtained from the AM2N90N test. Reasons for the different responses  
27 of CAM3LIU and AM2N90 to the change in the ice number concentrations are complicated  
28 because the modeled clouds and cloud microphysical properties also depend on other model  
29 processes, including the large-scale dynamic, thermodynamic, and hydrological processes. More  
30 in-depth analysis and further sensitivity tests to the parameters used in their microphysical  
31 schemes are needed to fully understand the differences in the CAM3LIU and AM2 simulated

1 clouds.

2

### 3 **5. Discussion and summary**

4 We have evaluated the mixed-phase cloud parameterizations used in the two major U.S.  
5 climate models, the NCAR CAM3 and GFDL AM2, in short-range forecasts under the DOE  
6 CCPP-ARM Parameterization Testbed (CAPT) against the in-situ and remote sensing data  
7 collected from the ARM M-PACE field experiment over the North Slope of Alaska. We have  
8 shown that both models are able to qualitatively capture the various cloud types observed during  
9 the M-PACE when they are initialized with realistic atmospheric conditions from the NWP  
10 analyses. However, there are significant differences in the simulated cloud fraction and cloud  
11 microphysical properties between the two models and between the models and the observations.  
12 CAM3 significantly underestimates the observed boundary layer cloud fraction and cannot  
13 realistically simulate the variations with temperature and cloud height of liquid water fraction in  
14 the total cloud condensate due to an oversimplified cloud microphysical scheme. It also largely  
15 overestimates the liquid water path for mid- and high level clouds. AM2 reasonably reproduces  
16 the observed boundary layer cloud fraction while its clouds contain much less cloud condensate  
17 than CAM3 and the observations. The simulation of the boundary layer mixed-phase clouds and  
18 their microphysical properties is considerably improved in CAM3 when a more physically based  
19 cloud microphysical scheme is used. The new scheme also leads to an improved simulation of  
20 the surface and top of the atmosphere longwave radiative fluxes. This study has shown that the  
21 Wegener-Bergeron-Findeisen process, i.e., the ice crystal growth by vapor deposition at the  
22 expense of coexisting liquid water, is important for the models to correctly simulate the  
23 characteristics of the observed microphysical properties in mixed-phase clouds.

24 Sensitivity tests have shown that these results are not sensitive to the initial data produced  
25 from two different NWP centers. Increasing model horizontal resolution helps better capture the  
26 subgrid-scale features for the Arctic frontal clouds but does not help improve the simulation of  
27 the single-layer boundary layer clouds. This might be because the low resolution climate models  
28 could reasonably resolve the single-layer boundary layer clouds, which uniformly covered a  
29 large area over NSA and its adjacent oceans during M-PACE. It is shown that AM2 simulated  
30 cloud fraction and LWP are sensitive to the change in ice number concentrations used in the  
31 Wegener-Bergeron-Findeisen process while CMA3LIU only shows moderate sensitivity in its

1 cloud fields to this change. Fully understanding the differences between AM2 and CAM3LIU  
2 requires more in depth analysis and further sensitivity tests. Reducing uncertainties in the  
3 measured IN number concentrations and ice crystals is also important to guide further model  
4 microphysics parameterization developments.

5 It has been shown that the model-produced single-layer boundary layer clouds have lower  
6 cloud top and cloud base than the observations. This can have a large impact on the surface and  
7 TOA radiation. This problem might be related to the low vertical resolution used in these climate  
8 models or deficiencies in the model boundary layer parameterizations. A study to examine the  
9 impact of increasing model vertical resolution and/or using an improved boundary layer  
10 parameterization on the simulated mixed-phase clouds is on-going. We will report the results  
11 from this study separately.

12  
13 **Acknowledgments.** The work reported here was funded by the US Department of Energy  
14 Atmospheric Radiation Measurement Program (ARM) and Climate Change Prediction Program  
15 (CCPP). The authors would like to thank the two anonymous referees for their valuable  
16 comments that helped to clarify and improve the paper. We gratefully thank Drs. G. McFarquhar,  
17 D. Turner, Z. Wang, C. Long, and P. Minnis for making the M-PACE field campaign data  
18 available for our use. Special thanks go to Dr. R. McCoy for providing the aircraft data in a  
19 format that can be easily used for model evaluation. We thank Prof. Eugene Clothiaux and Karen  
20 Johnson for their help on deriving the cloud fraction from ARSCL products. We thank all the  
21 LLNL CAPT team members for their valuable comments on this work. The Climate Data  
22 Analysis Tools (CDAT) that were developed in the Program for Climate Model Diagnosis and  
23 Intercomparison (PCMDI) were used to perform our analyses. This research was performed  
24 under the auspices of the U. S. Department of Energy, Office of Science, Office of Biological  
25 and Environmental Research by the University of California, Lawrence Livermore National  
26 Laboratory, under contract W-7405-Eng-48. The Pacific Northwest National Laboratory is  
27 operated for the DOE by Battelle Memorial Institute under contract DE-AC06-76RLO 1830.

28

29

## 1 **References**

- 2
- 3 ACIA (2004), Impacts of a Warming Arctic: Arctic Climate Impact Assessment. Cambridge  
4 University Press, 1020 pp.
- 5 Bigg, E. K. (1996), Ice forming nuclei in the high Arctic, *Tellus*, 48, 223-233.
- 6 Bergeron, T., (1935), On the physics of clouds and precipitation, *Proces Verbaux de*  
7 *l'Association de Meteorologie*, International Union of Geodesy and Geophysics, 156-178.
- 8 Boyle, J. S. and 8 co-authors (2005), Diagnosis of Community Atmospheric Model 2 (CAM2) in  
9 numerical weather forecast configuration at the Atmospheric Radiation Measurement  
10 sites, *J. Geophys. Res.*, 110, D15S15, doi:10.1029/2004JD005042.
- 11 Byran, A., P. Rasch, J. Hack, and J. McCaa (2006), Representation of clouds and precipitation  
12 processes in the Community Atmosphere Model Version 3 (CAM3), *J. Climate*, 19, 2184  
13 – 2198.
- 14 Clothiaux, E. E., et al. (2000), Objective determination of cloud heights and radar reflectivities  
15 using a combination of active remote sensors at the ARM CART sites. *J. Appl. Meteor.*,  
16 39, 645-665.
- 17 Collins, W. D., and co-authors (2006), The formulation and atmospheric simulation of the  
18 Community Atmosphere Model Version 3 (CAM3), *J. Climate*, 19, 2144-2161.
- 19 Cotton, W. R., G. J. Tripoli, R. M. Rauber, and E. A. Mulvihill (1986), Numerical simulation of  
20 the effects of varying ice crystal nucleation rates and aggregation processes on orographic  
21 snowfall, *J. Climate Appl. Meteor.*, **25**, 1658–1680.
- 22 Curry, J. A., W. B. Rossow, D. Randall, and J. L. Schramm (1996), Overview of Arctic cloud  
23 and radiation characteristics. *J. Climate*, 9, 1731-1764.
- 24 Curry, J. A., and Coauthors (2000), FIRE Arctic Clouds Experiment. Overview of Arctic cloud  
25 and radiation properties. *Bull. Amer. Meteor. Soc.*, 81, 5-29.
- 26 Findeisen, W. (1938), Kolloid-meteorologische Vorgänge bei Neiderschlags-bildung. *Meteor. Z.*,  
27 55, 121-133.
- 28 Fridlind, A. M. and Coauthors (2007), Ice properties of single-layer stratocumulus during the  
29 Mixed-Phase Arctic Cloud Experiment (M-PACE): Part II, Model results, *J. Geophys.*  
30 *Res.*, in press.
- 31 Fowler, L. D. D. A. Randall, and S. A. Rutledge, 1996, Liquid and ice cloud microphysics in the

1 CSU general circulation model. Part I: Model description and simulated microphysical  
2 processes. *J. Climate*, 9, 489-529.

3 Fu, Q., and S. Hollars (2004), Testing mixed-phase cloud water vapor parameterizations with  
4 SHEBA/FIRE-ACE observations, *J. Atmos. Sci.*, **61**, 2083–2091.

5 Gettelman, A., H. Morrison, and S. J. Ghan (2007), A new two-moment bulk stratiform cloud  
6 microphysics scheme in the Community Atmosphere Model (CAM3), Part II: Single-  
7 column and global results, *J. Climate* (submitted)

8 The GFDL Global Atmospheric Model Development Team (2004), The new GFDL global  
9 atmosphere and land model AM2-LM2: Evaluation with prescribed SST simulations, *J.*  
10 *Clim.*, 17, 4641-4673.

11 Gregory, D. and D. Morris (1996), The sensitivity of climate simulations to the specification of  
12 mixed phase clouds, *Climate Dynamics*, 12, 641-651.

13 Hobbs, P. V., and A. L. Rangno (1998), Microstructures of low and middle-level clouds over the  
14 Beaufort sea. *Quart. J. Roy. Meteor. Soc.*, 124, 2035-2071.

15 Isaac, G. A., and Coauthors (2001), Recent Canadian research on aircraft in-flight icing. *Can.*  
16 *Aeronaut. Space. J.*, 47, 213-221.

17 Isaac, G. A., and Coauthors (2005), First results from the Alliance Icing Research Study II.  
18 Preprints, *AIAA 43d Aerospace Science Meeting and Exhibit*, AIAA 2005-0252, Reno,  
19 NV, American Institute of Aeronautics and Astronautics, 1-18.

20 Klein, S. A., and C. Jakob (1999), Validation and sensitivities of frontal clouds simulated by the  
21 ECMWF model, *Mon. Wea. Rev.*, 127, 2514-2531.

22 Korolev A., and G. A. Isaac (2006), Relative humidity in liquid, mixed-phase, and ice clouds,  
23 Validation and sensitivities of frontal clouds simulated by the ECMWF model, *J. Atmos.*  
24 *Sci.*, **63**, 2865–2880.

25 Li, Z.-X. and H. Le Treut (1992), Cloud-radiation feedbacks in a general circulation model and  
26 their dependence on cloud modeling assumptions, *Climate Dyn.*, 7, 133-139.

27 Liu, X. and J. E. Penner (2005), Ice nucleation parameterization for global models,  
28 *Meteorologische Zeitschrift* 14, No. 4, 499-514.

29 Liu, X. J. E. Penner, S. Ghan, and M. Wang (2007a), Inclusion of ice microphysics in the NCAR  
30 Community Atmospheric Model version 3 (CAM3), *J. Climate*, 20, 4526-4547.

31 Liu, X., S. Xie, and S. Ghan (2007b), Evaluation of a New Mixed-Phase Cloud Microphysics

1 Parameterization with CAM3 Single-Column Model and M-PACE Observations,  
2 *Geophys. Res. Lett.* in press,

3 Lohmann, U. (2002), Possible aerosol effects on ice clouds via contact nucleation, *J. Atmos. Sci.*,  
4 **59**, 647–656.

5 McFarquhar, G. M., and co-authors (2007), Ice properties of single layer boundary clouds during  
6 the Mixed-Phase Arctic Cloud Experiment (MPACE): Part I: Observations, *J. Geophys.*  
7 *Res.*, in press.

8 Ming, Y. and co-authors (2007), Modeling the interactions between aerosols and liquid water  
9 clouds with a self-consistent cloud scheme in a general circulation model, *J. Atmos. Sci.*,  
10 **64**, 1189–1209.

11 Morrison, H., and A. Gettelman, (2007), A new two-moment bulk stratiform cloud microphysics  
12 scheme in the Community Atmosphere Model (CAM3), Part I: Description and  
13 numerical tests, *J. Climate* (submitted)

14 Perovich, D. K., and Coauthors (1999), Year on ice gives climate insights. *Eos, Trans. Amer.*  
15 *Geophys. Union*, **80**, 481.

16 Phillips, T. J. and 9 co-authors (2004), Evaluating parameterizations in GCMs: Climate  
17 simulation meets weather prediction, *Bull. Am. Meteorol. Soc.*, **85**, 1903-1915.

18 Pinto, J. O. (1998), Autumnal mixed-phase cloudy boundary layers in the Arctic, *J. Atmos. Sci.*,  
19 **55**, 2016-2038.

20 Prenni, A. J. and 8 co-authors (2007), Can ice-nucleating aerosols affect Arctic seasonal climate?  
21 *Bull. Am. Meteorol. Soc.* **88**, 541-550.

22 Rasch, P. J., and J. E. Kristjánsson (1998), A comparison of the CCM3 model climate using  
23 diagnosed and predicted condensate parameterizations. *J. Climate*, **11**, 1587-1614.

24 Rotstayn, L. D. (1997), A physical based scheme for the treatment of stratiform clouds and  
25 precipitation in large-scale models. I: Description and evaluation of the microphysical  
26 processes, *Q. J. R. Meteorol. Soc.* **123**, 1227-1282.

27 Rotstayn, L. D., B. F. Ryan, and J. J. Katzfey (2000), A scheme for calculation of the liquid  
28 fraction in mixed-phase stratiform clouds in large-scale models, *Mon. Wea. Rev.*, **128**,  
29 1070-1088.

30 Sud, Y. C., D. M. Mocko, and S. J. Lin (2006), Performance of two cloud-radiation  
31 parameterization schemes in the finite volume general circulation model for anomalously

1 wet May and June 2003 over the continental United States and Amazonia. *J. Geophys.*  
2 *Res.*, **111**, D06201, doi:10.1029/2005JD006246.

3 Tiedtke, M.(1993), Representation of clouds in large-scale models. *Mon. Wea. Rev.*, *121*, 3040-  
4 3061.

5 Turner, D.D., S.A. Clough, J.C. Liljegren, E.E. Clothiaux, K. Cady-Pereira, and K.L. Gaustad,  
6 (2007), Retrieving liquid water path and precipitable water vapor from Atmospheric  
7 Radiation Measurement (ARM) microwave radiometers. *IEEE Trans. Geosci. Remote*  
8 *Sens.*, *submitted*.

9 Uttal, T. et al. (2002), Surface heat budget of the Arctic Ocean. *Bull. Amer. Meteor. Soc.*, **83**,  
10 255-275.

11 Verlinde, J. and Coauthors (2007), The Mixed-Phase Arctic Cloud Experiment, *Bull. Am.*  
12 *Meteorol. Soc.*, *88*, 205-221.

13 Wang, Z. (2007), Refined two-channel microwave radiometer liquid water path retrieval at cold  
14 regions by using multiple-sensor measurements, *IEEE Geoscience and Remote Sensing*  
15 *Letters*, **4**, 591-595.

16 Wegener, A. (1911), *Thermodynamik der Atmosphäre*. Leipzig, 331pp.

17 Williamson, D. L., and co-authors (2005), Moisture and temperature balances at the Atmospheric  
18 Radiation Measurement Southern Great Plains Site in forecasts with the Community  
19 Atmosphere Model (CAM2), *J. Geophys. Res.*, *110*, D15S16,  
20 doi:10.1029/2004JD005109.

21 Vavrus, S. (2004), The impact of cloud feedbacks on Arctic climate under greenhouse forcing. *J.*  
22 *Climate*, *17*, 603-615.

23 Xie, S. M. Zhang, J. S. Boyle, R. T. Cederwall, G. L. Potter, and W. Lin (2004), Impact of a  
24 revised convective triggering mechanism on Community Atmosphere Model, Version 2,  
25 simulations: Results from short-range weather forecasts, *J. Geophys. Res.*, *109*, D14102,  
26 doi:10.1029/2004JD004692.

27 Xie, S. C., and Coauthors (2005), Simulations of midlatitude frontal clouds by single-column and  
28 cloud-resolving models during the Atmospheric Radiation Measurement March 2000 cloud  
29 intensive operational period. *J. Geophys. Res.*, *110*, D15S03, doi:10.1029/2004JD005119.

30 Xie, S., S. A. Klein, J. J. Yio, A. C. M. Beljaars, C. N. Long, and M. Zhang (2006), An

1 assessment of ECMWF analyses and model forecasts over the North Slope of Alaska using  
2 observations from the ARM Mixed-Phase Arctic Cloud Experiment, *J. Geophys. Res.*, 111,  
3 D05107, doi:10.1029/2005JD006509.

4 Zhang, M., W. Lin, C. Bretherton, J. Hack, and P. Rasch (2003), A modified formulation of  
5 fractional stratiform condensation rate in the NCAR Community Atmospheric Model  
6 (CAM2), *J. Geophys. Res.*, 108, 4035, doi:10.1029/2002JD002523.

7 Zhang, M. H., and Coauthors (2005), Comparing clouds and their seasonal variations in 10  
8 atmospheric general circulation models with satellite measurements, *J. Geophys. Res.*, 110,  
9 D15S01, doi:10.1029/2005JD005923.

10

## 1 **Figure Captions**

2  
3 **Figure 1.** Time-height cross sections of ARSCL cloud frequency (a) and modeled cloud fraction  
4 (b) CAM3, (c) AM2, and (d) CAM3LIU at Barrow during M-PACE. The unit is %.

5 **Figure 2.** Time series of the total ARSCL cloud frequency and modeled cloud fraction. Black  
6 line with dots is for ARSCL, Red line is for CAM3, green for CAMLIU, and blue for  
7 AM2. The unit is %.

8 **Figure 3.** Time-height cross sections of model-produced liquid water mixing ratio (g/kg). (a)  
9 CAM3, (b) AM2, and (c) CAM3LIU. The solid lines in the figures are model-  
10 simulated temperatures.

11 **Figure 4.** Same as Figure 3 except for ice water mixing ratio (g/kg).

12 **Figure 5.** Time series of the observed and model-produced (a) cloud liquid water path (g/m<sup>2</sup>)  
13 and (b) ice water path (g/m<sup>2</sup>) during M-PACE. The black solid line with dots is from  
14 Turner's retrievals and + is from Wang's retrievals. Red lines are for CAM3, green for  
15 CAMLIU, and blue for AM2.

16 **Figure 6.** Liquid fraction as a function of cloud height. (a) UND citation data, (b) CAM3, (c)  
17 AM2, and (d) CAM3LIU. Different color dots in (a) represent data collected from  
18 different flights. Note that the cloud altitude in the figure is normalized from 0 at cloud  
19 base to 1 at cloud top.

20 **Figure 7.** Liquid fraction as a function of temperature. (a) UND citation data, (b) CAM3, (c)  
21 AM2, and (d) CAM3LIU. Different color dots in (a) represent data collected from  
22 different flights.

23 **Figure 8.** Time series of the observed and model-produced (a) surface downwelling longwave  
24 radiative fluxes (W/m<sup>2</sup>) and (b) TOA outgoing longwave radiative fluxes (W/m<sup>2</sup>).  
25 Black lines are observations. Red lines are for CAM3, green for CAMLIU, and blue  
26 for AM2.

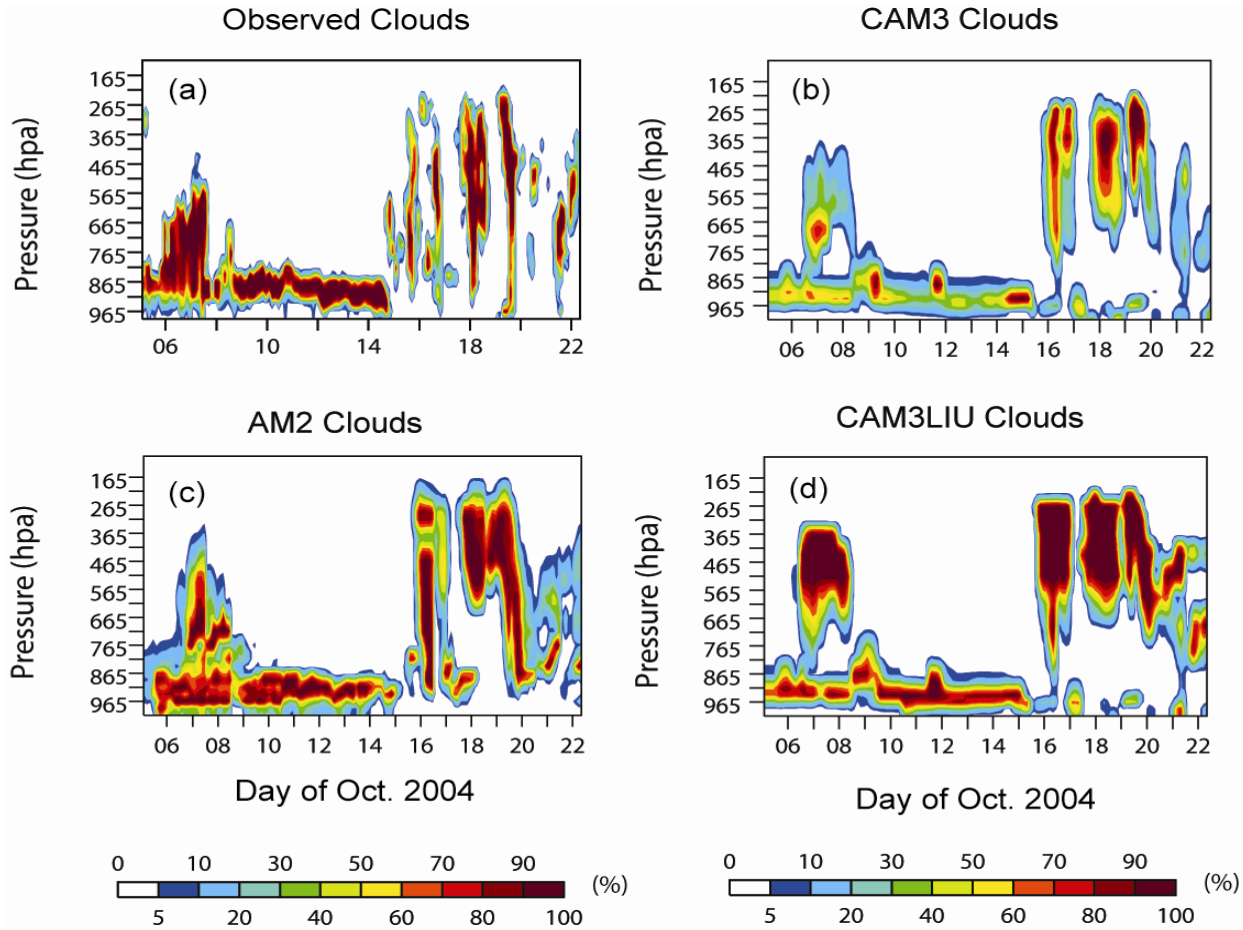
27 **Figure 9.** Same as Figure 1 except for (a) AM2N90 and (b) AM2N90N.

28 **Figure 10.** Same as Figure 5 except that red line is for AM2, green for AM2N90, and blue for  
29 AM2N90N.

30 **Figure 11.** Same as Figure 1 except for CAM3LIUN

31 **Figure 12.** Same as Figure 5 except that red line is for CAM3LIU and blue for CAM3LIUN.

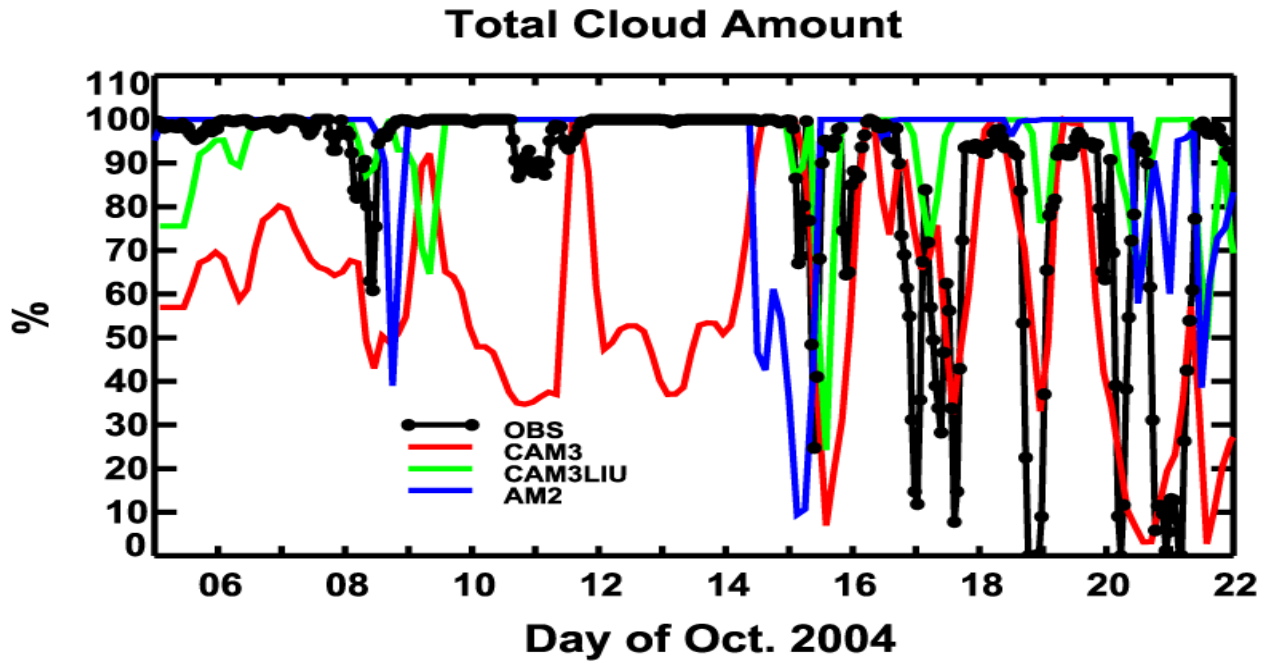
1  
2  
3



4  
5  
6  
7  
8  
9  
10

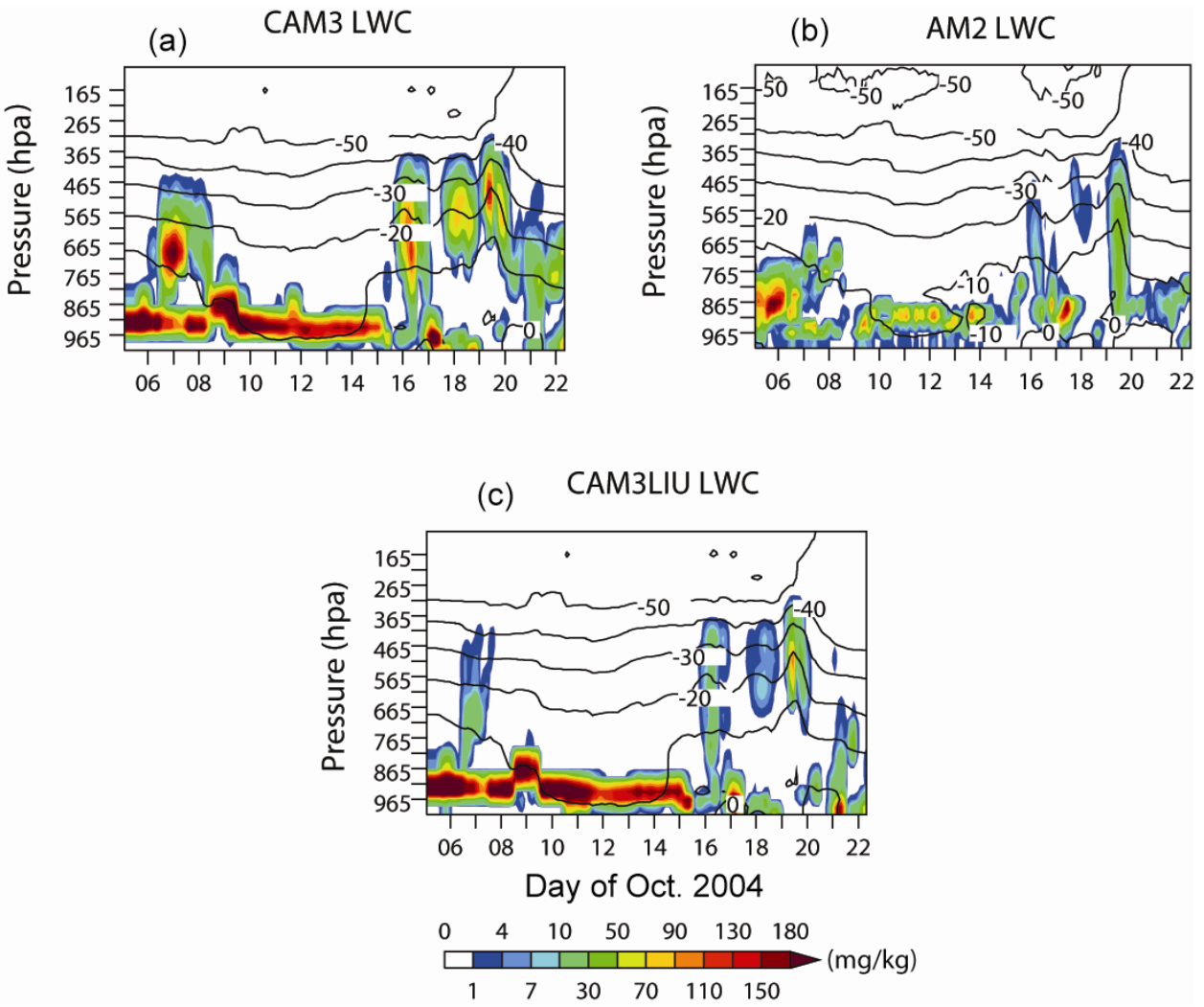
**Figure 1.** Time-height cross sections of ARSCL cloud frequency (a) and modeled cloud fraction (b) CAM3, (c) AM2, and (d) CAM3LIU at Barrow during M-PACE. The unit is %.

1  
2



3  
4  
5  
6  
7

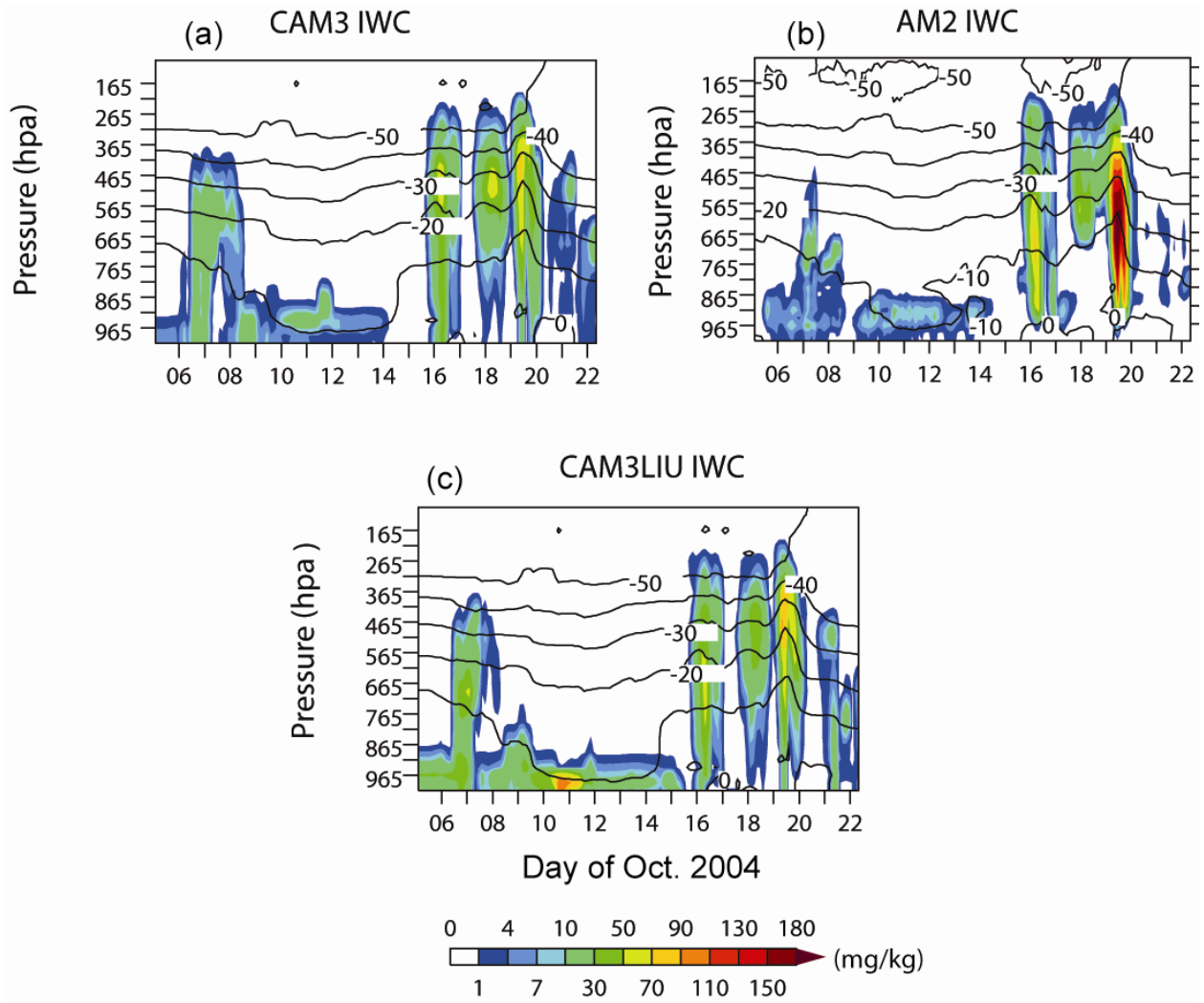
**Figure 2.** Time series of the total ARSCL cloud frequency and modeled cloud fraction. Black line with dots is for ARSCL, Red line is for CAM3, green for CAMLIU, and blue for AM2. The unit is %.



1  
2  
3  
4  
5  
6

**Figure 3.** Time-height cross sections of model-produced liquid water mixing ratio (g/kg). (a) CAM3, (b) AM2, and (c) CAM3LIU. The solid lines in the figures are model-simulated temperature.

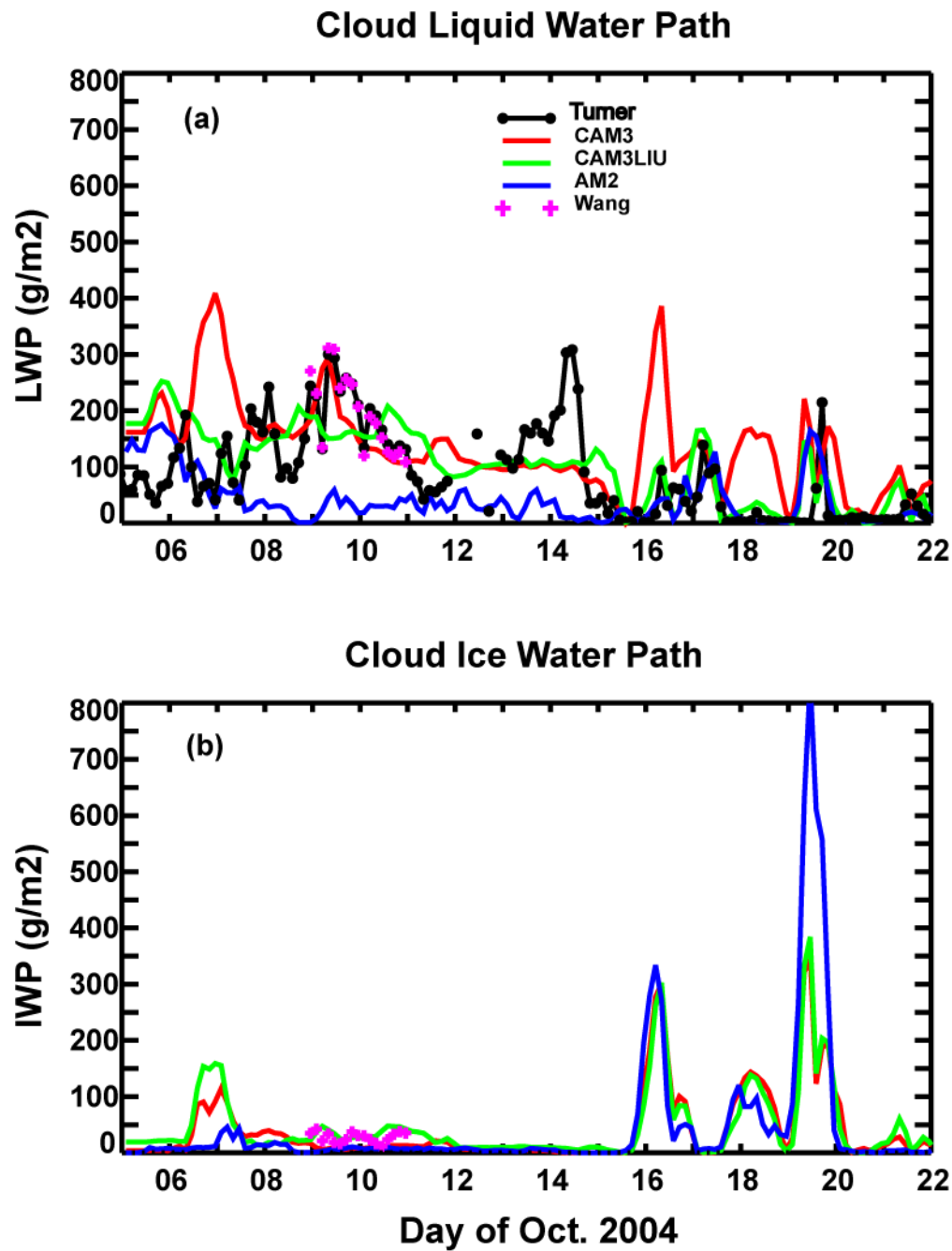
1



2

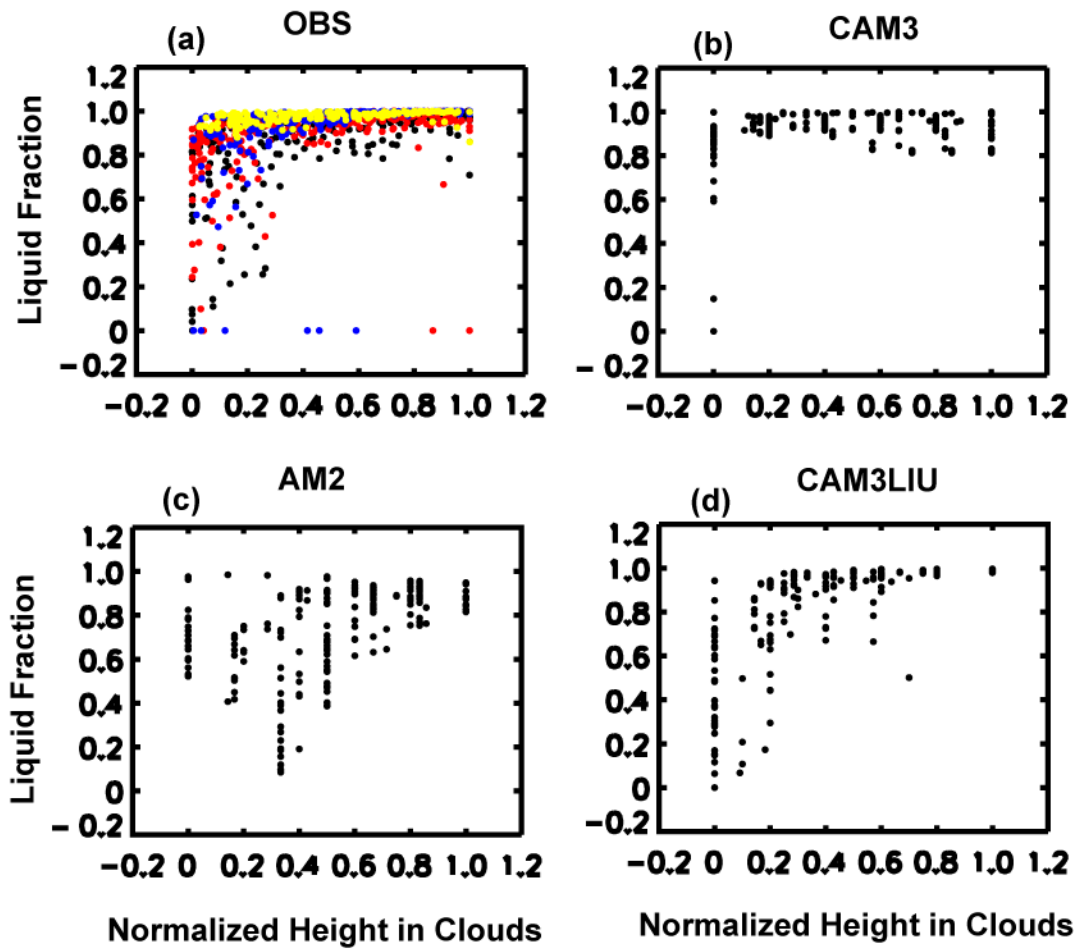
3

4 **Figure 4.** Same as Figure 3 except for ice water mixing ratio (g/kg).



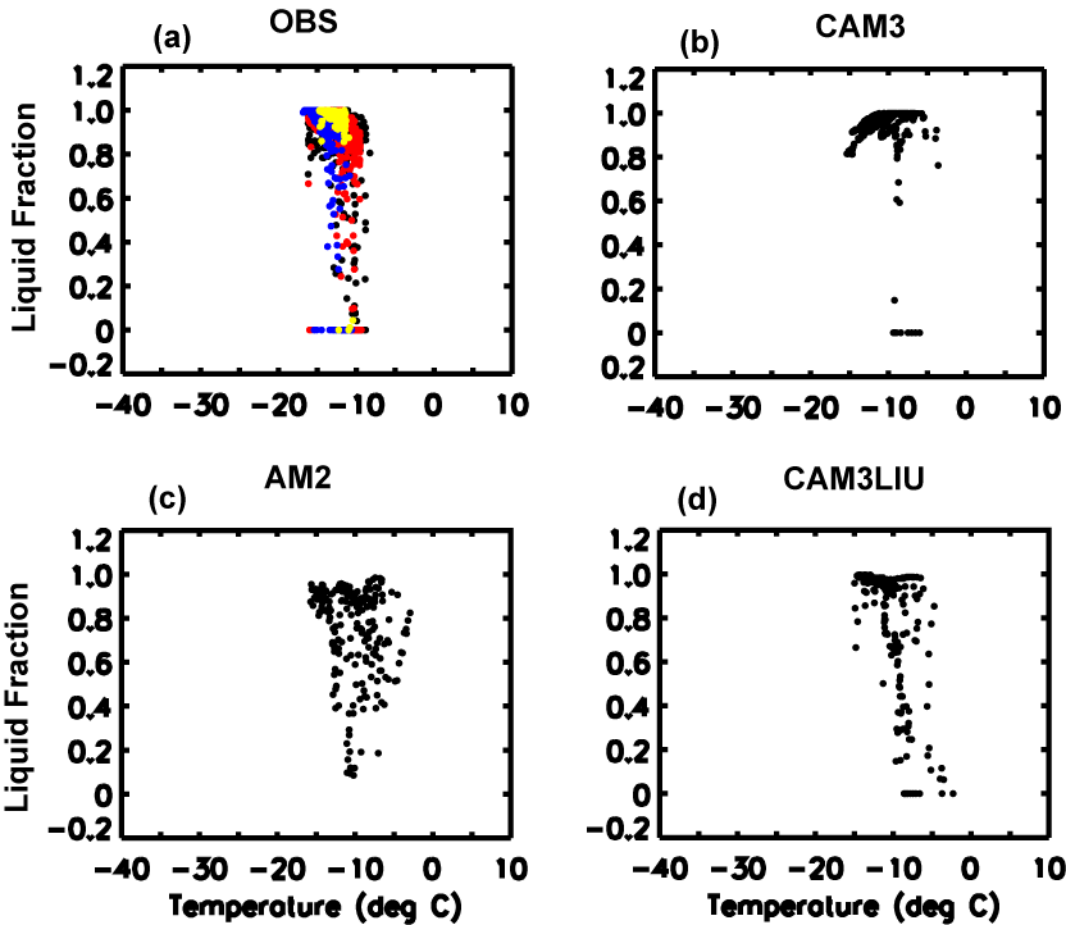
1  
2  
3  
4  
5  
6  
7

**Figure 5.** Time series of the observed and model-produced cloud liquid water path (g/m<sup>2</sup>) and ice water path (g/m<sup>2</sup>) during M-PACE. Black solid line with dots is from Turner’s retrievals and + is from Wang’s retrievals. Red lines are for CAM3, green for CAMLIU, and blue for AM2.



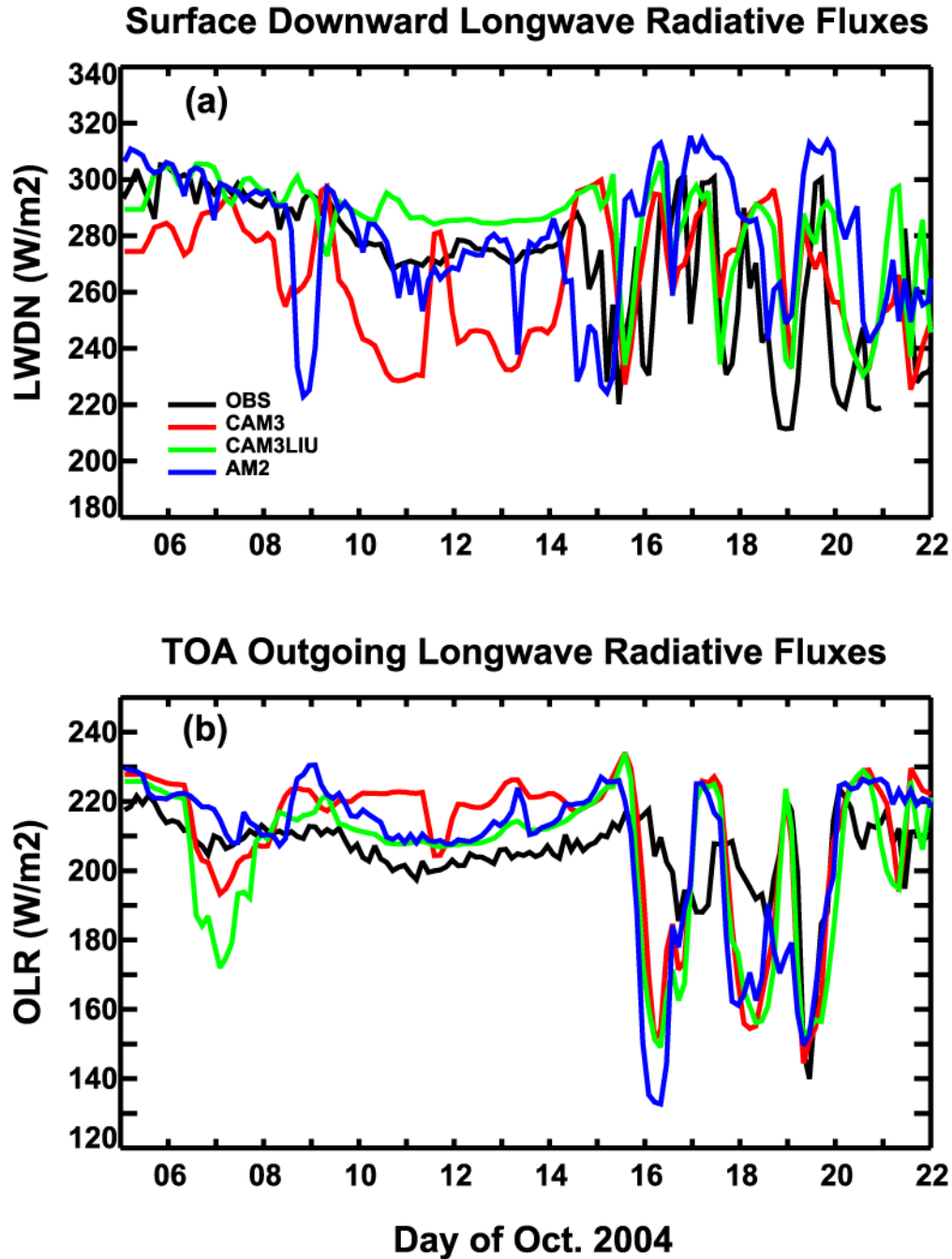
1  
2  
3  
4  
5  
6  
7

**Figure 6.** Liquid fraction as a function of cloud height. (a) UND citation data, (b) CAM3, (c) AM2, and (d) CAM3LIU. Different color dots in (a) represent data collected from different flights. Note that the cloud altitude in the figure is normalized from 0 at cloud base to 1 at cloud top.



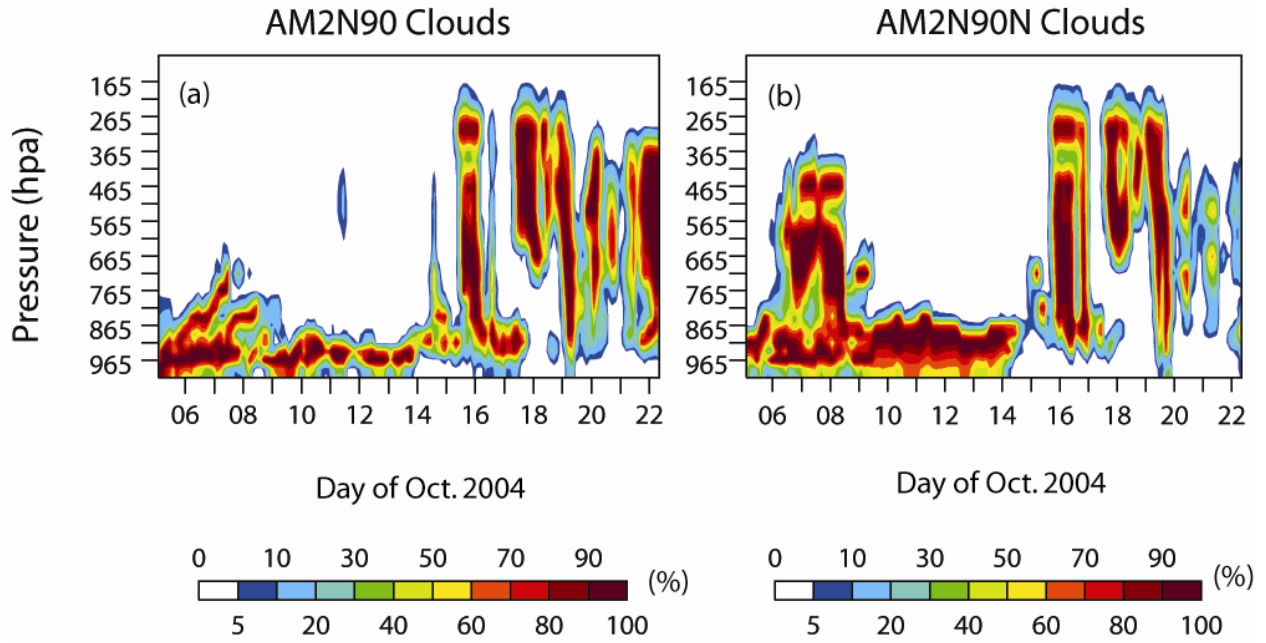
1  
 2  
 3  
 4  
 5  
 6  
 7

**Figure 7.** Liquid fraction as a function of temperature. (a) UND citation data, (b) CAM3, (c) AM2, and (d) CAM3LIU. Different color dots in (a) represent data collected from different flights.



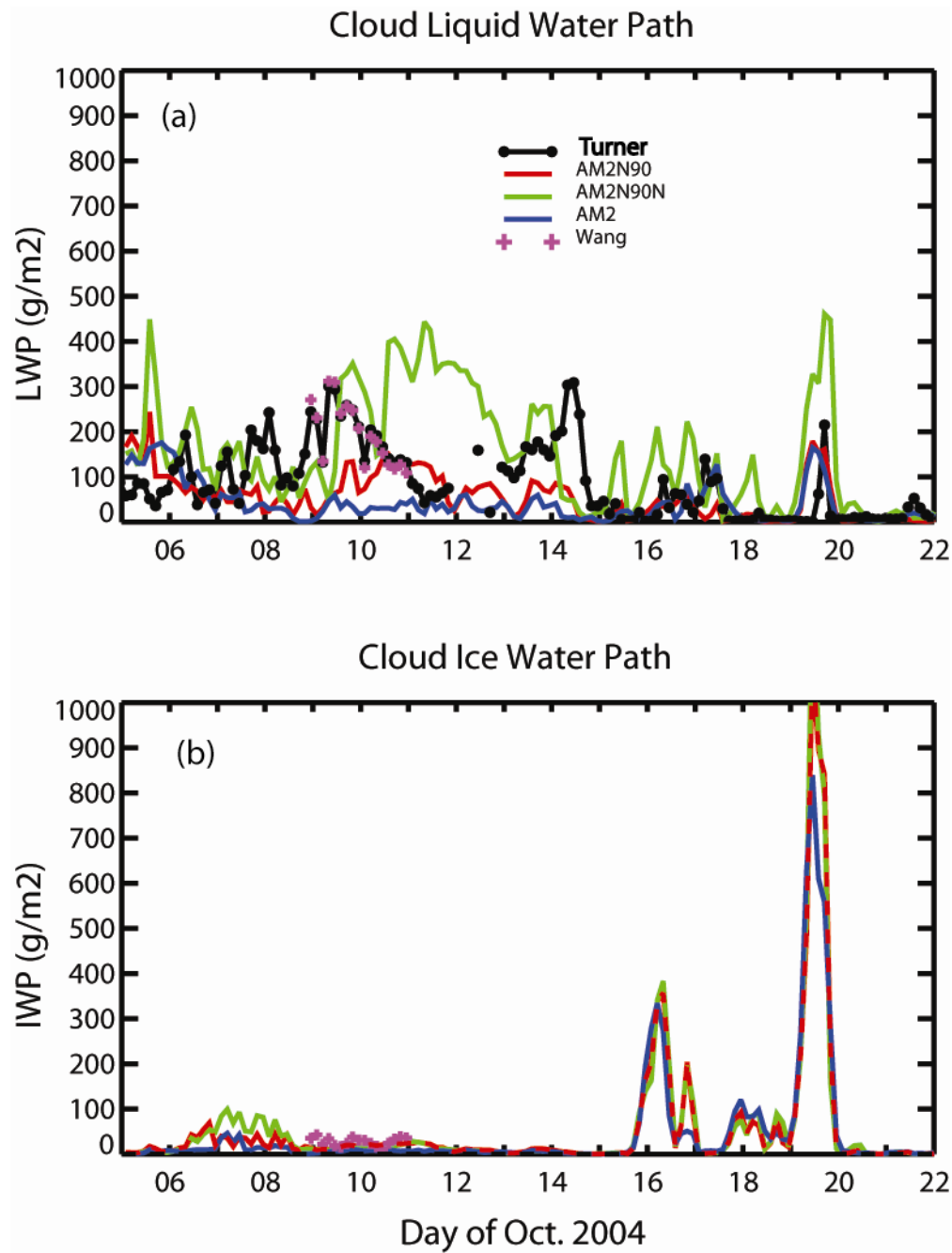
1  
2  
3  
4  
5  
6

**Figure 8.** Time series of the observed and model-produced (a) surface downwelling longwave radiative fluxes (W/m<sup>2</sup>) and (b) TOA outgoing longwave radiative fluxes (W/m<sup>2</sup>). Black lines are observations. Red lines are for CAM3, green for CAMLIU, and blue for AM2.



1  
2  
3  
4  
5

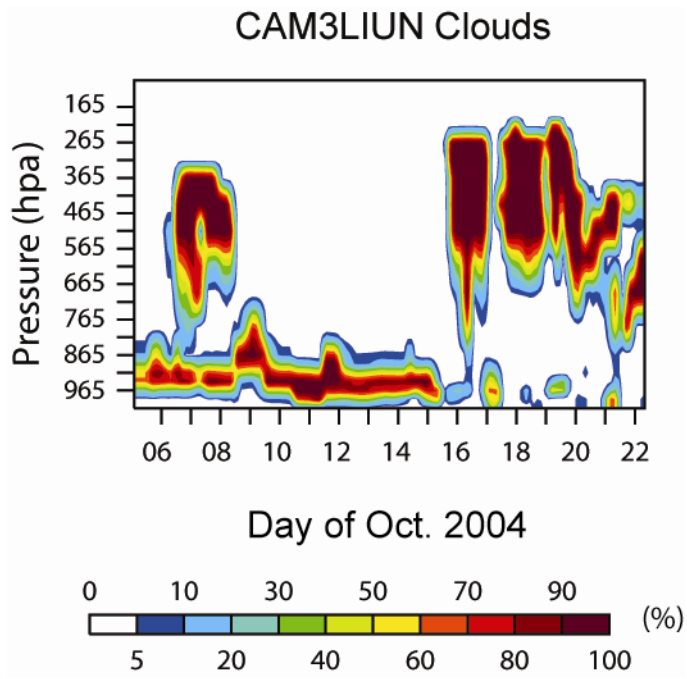
**Figure 9.** Same as Figure 1 except for (a) AM2N90 and (b) AM2N90N.



1  
2  
3  
4  
5  
6  
7  
8

**Figure 10.** Same as Figure 5 except that red line is for AM2, green for AM2N90, and blue for AM2N90N.

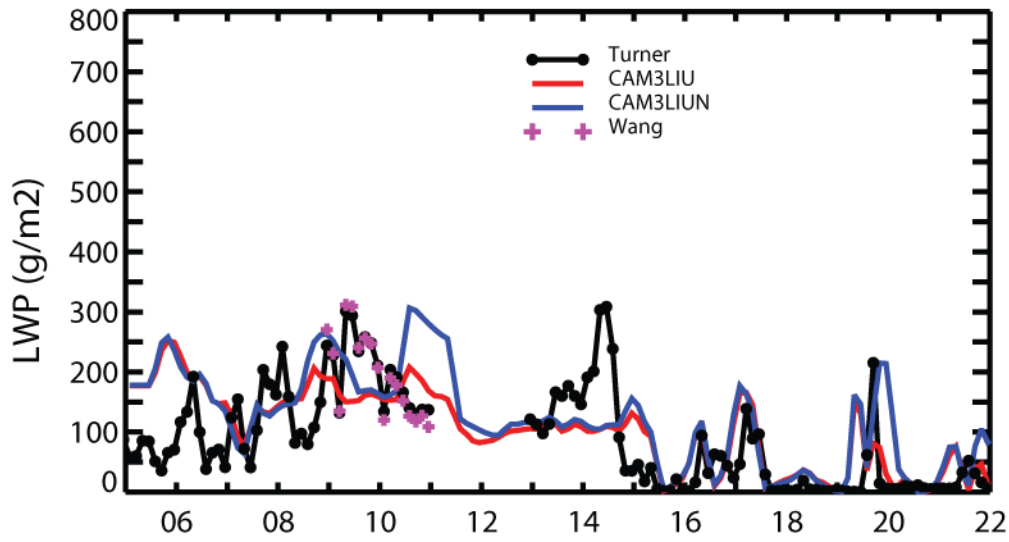
1  
2



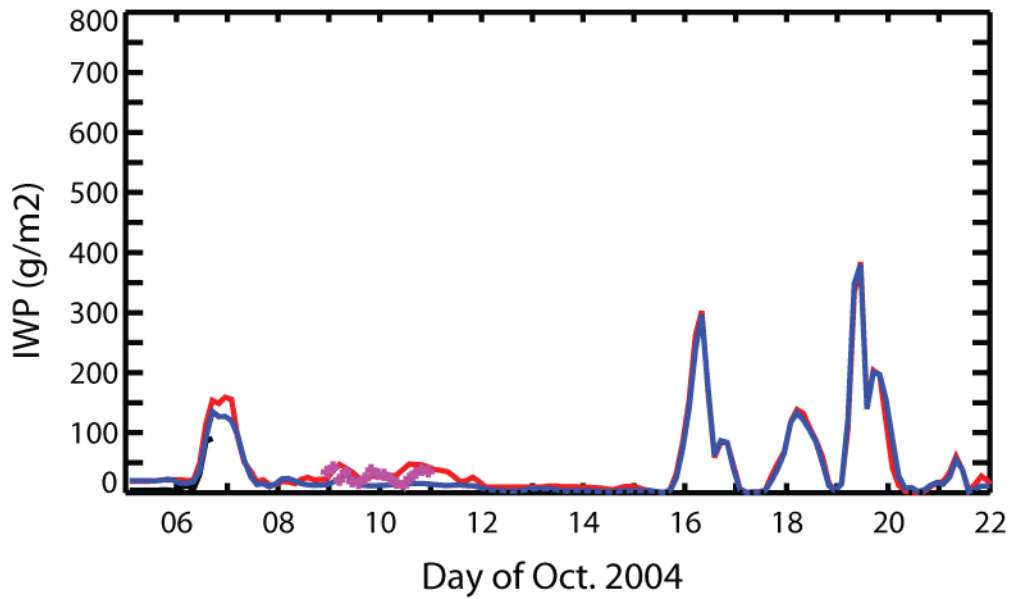
3  
4  
5

**Figure 11 Same as Figure 1 except for CAM3LIUN**

### Cloud Liquid Water Path at Barrow



### Cloud Ice Water Path at Barrow



1  
2  
3  
4

**Figure 12.** Same as Figure 5 except that red line is for CAM3LIU and blue for CAM3LIUN.